YGS Open File 2025-3

Preliminary observations from four reduced intrusion-related gold deposits, Selwyn basin, Yukon

S.H.M. Ellis

Yukon

Published under the authority of the Department of Energy, Mines and Resources, Government of Yukon https://yukon.ca/en/department-energy-mines-resources.

Publié avec l'autorisation du Ministères de l'Énergie, des Mines et des Ressources du gouvernement du Yukon, https://yukon.ca/en/department-energy-mines-resources.

This, and other Yukon Geological Survey publications, may be obtained from:

Yukon Geological Survey
102-300 Main Street
Box 2703 (K-102)
Whitehorse, Yukon, Canada Y1A 2C6

email geology@gov.yk.ca

Visit the Yukon Geological Survey website at https://yukon.ca/en/science-and-natural-resources/geology.

In referring to this publication, please use the following citation:

Ellis, S.H.M., 2025. Preliminary observations from four reduced intrusion-related gold deposits, Selwyn basin, Yukon. Yukon Geological Survey, Government of Yukon, Open File 2025-3, 46 p. plus appendices.

Front cover: Photomicrograph at 20X of gold with pyrrhotite and molybdenum in reflected light at the Valley deposit, Yukon. Photo credit: Sarah Ellis, Yukon Geological Survey.

Yukon

YGS Open File
2025-3

Preliminary observations from four reduced intrusion-related gold deposits, Selwyn basin, Yukon

Sarah H.M. Ellis
Yukon Geological Survey

Table of Contents

Abstract

Host rocks, veins and alteration in reduced intrusion-related gold (RIRG) deposits display similar features and distribution across the Tombstone gold belt (TGB). The primary intrusive rocks hosting gold at these deposits are felsic to intermediate, silica-saturated, alkalic to calcic, metaluminous to weakly peraluminous magnesian (calc-alkaline) granodiorite, quartz-monzonite, monzonite and syenite. Preliminary field and petrographic observations suggest that distribution of veins, vein textures, and their correlative vein selvedge alteration assemblages show similar distribution patterns to porphyry deposit models on a more spatially restricted but observable (drill core) scale. At each of the deposits examined on four properties, sulphide-poor (3–5% sulphide minerals) quartz veins were commonly observed proximal to the causative intrusion, whereas sulphide-rich (>10% sulphide minerals) veins tend to be more distal, though are commonly observed using the same fluid pathways as earlier veins. Early sulphide-poor quartz veins commonly exhibit potassic and locally sodic alteration in vein selvedges, whereas sulphide-rich veins typically coincide with phyllic (sericitic) alteration. Sinuous veins with diffuse boundaries suggest emplacement within a higher temperature ductile regime closer to the centre of the mineralizing intrusion, whereas sharp, straight-sided quartz sulphide-rich veins are more typical and emplaced within a moderate temperature brittle regime in the intrusion carapace and hornfelsed country rocks.

Plain language summary

Reduced intrusion-related gold deposits are a type of gold deposit related to 98 to 90 Ma intrusive rocks emplaced across a region known as the Tombstone gold belt (TGB) in east-central Yukon (Hart, 2007). The model for this type of mineral system is primarily based on deposit research in the Yukon and east-central Alaska in the 1990s to early 2000s. The past-producing Eagle Gold and Brewery Creek mines are examples of these types of deposits. There have been several new discoveries since 2021 within the TGB which have led to a significant interest in exploration for these types of deposits. This project characterizes the host rocks, veins and hydrothermal alteration of four RIRG deposits across the TGB with the goal of better understanding controls on gold mineralization. Preliminary findings from this research show that sinuous quartz veins occur close to the intrusions and straight-sided quartz veins occur farther away. Similarly, the abundance of sulphide (and gold) in the veins varies with distance from the intrusion. Both of these observations have important implications for exploration.

Introduction

Reduced intrusion-related gold (RIRG) deposits are coeval with and genetically linked to felsic to intermediate mid-Cretaceous ilmenite and titanite-bearing intrusions (Baker and Lang, 2001; Selby et at., 2003; Hart et al., 2004; Hart, 2007). In the Yukon, these deposits are best recognized within the Selwyn basin region and are associated with plutonic rocks of the Tombstone, Mayo and Tungsten suites (Colpron et al., 2016). This belt of magmatic rocks, and associated deposits, are commonly referred to as the Tombstone-Tungsten belt or the Tombstone gold belt (TGB). The TGB extends approximately 1000 km from southwestern Northwest Territories, across central Yukon to the Tintina fault, where it is offset into east-central Alaska (Fig. 1). The TGB represents the innermost mid-Cretaceous (104–90 Ma) plutonic belt of the northern Cordillera with intrusions emplaced broadly parallel to the ancient North American continental margin (Fig. 2; Hart et al., 2004).

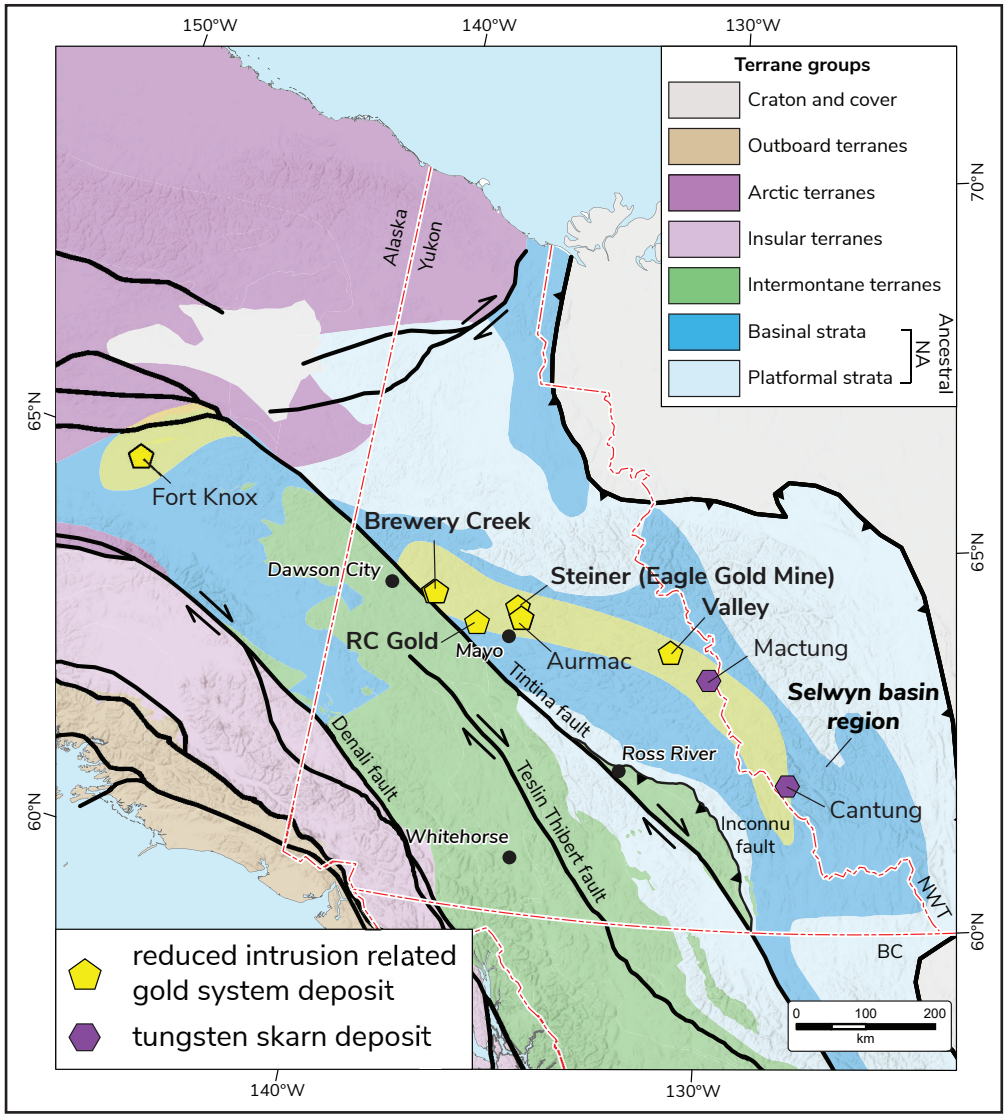

Figure 1. *Simplified terrane map of the Yukon, northern British Columbia and eastern Alaska. Regional faults, significant reduced intrusion-related gold system deposits (gold, tungsten), Selwyn basin region, and the location of the Tombstone gold belt (denoted by yellow polygon) are illustrated. Note: Brewery Creek hosts the Reserve trend and Classic zone deposits, RC Gold hosts the Blackjack and Eiger deposits. Terrane map modified from Colpron and Nelson (2011). Deposits from Yukon MINFILE (2024).*

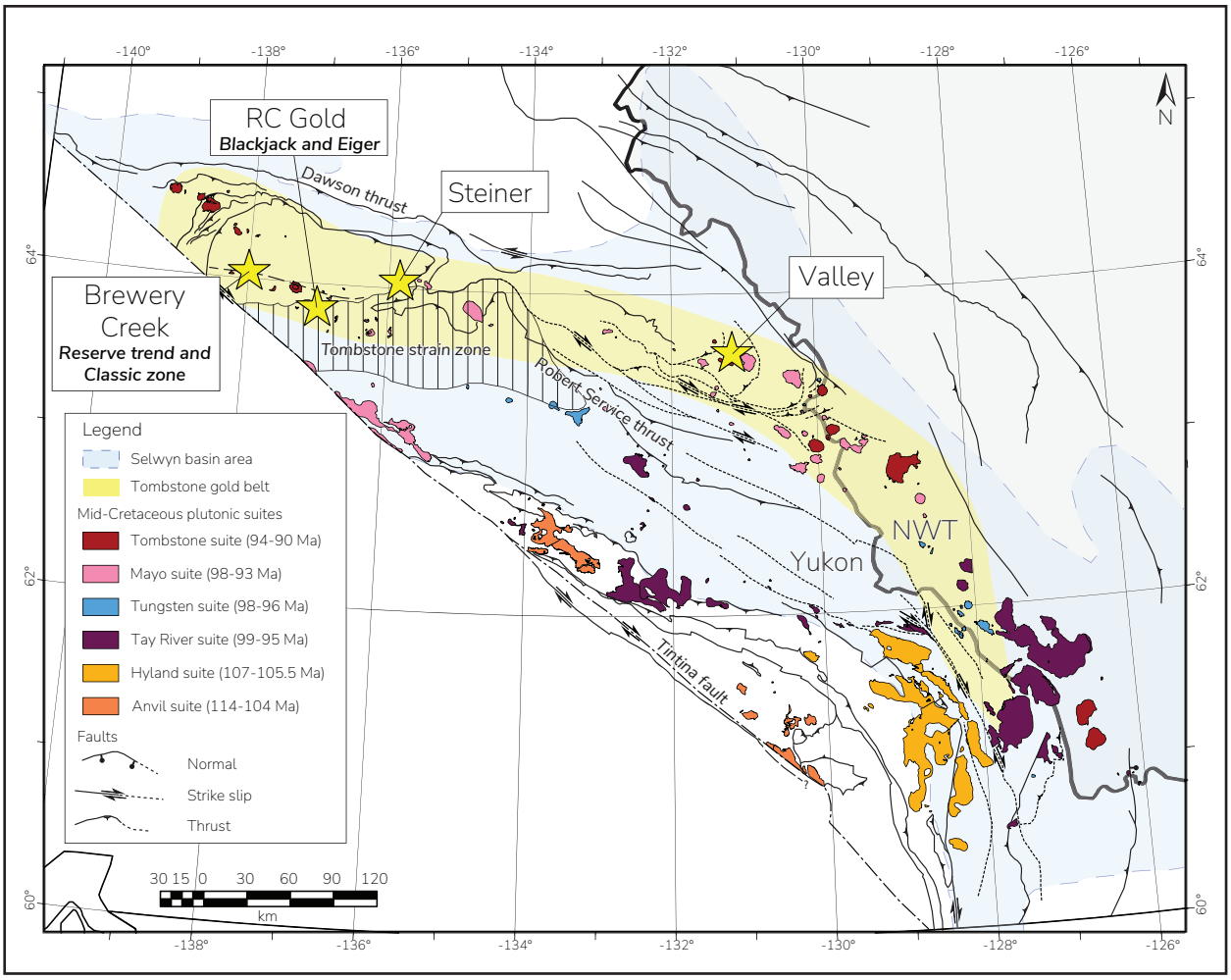

Figure 2. *Distribution of mid-Cretaceous plutonic suites and Cretaceous faulting across the Selwyn basin region (D. Moynihan, pers. comm., 2024). Yellow stars indicate the locations of deposits that are part of this study.*

Reduced intrusion-related gold deposits are recognized as part of larger reduced intrusion-related gold systems (RIRGS) that include tungsten skarn, silver-zinc-lead vein and varying styles of gold mineralization. These systems are best developed in and adjacent to, <1 km cylindrical-shaped plutons that intrude metasedimentary rocks (Hart, 2007). Reduced intrusion-related gold deposits typically lack stockwork veins and broad alteration footprints as seen in typical porphyry settings. The lack of these features led previous researchers to interpret that pluton emplacement depth is an important control on the style of mineralization (Hart, 2007). The deeper emplacement depths and absence of significant volumes of meteoric water suggest that fluid flow and mineralization are heavily influenced by the pre and syn-mineralization structural regime as established by Hart et al., (2000), Stephens et al., (2000, 2004) and Mair et al., (2006).

The recent discoveries and deposit definition of RIRG deposits (e.g., Valley, AurMac, Blackjack and Eiger deposits) across the TGB has initiated a resurgence in gold exploration activity in the Selwyn basin region. The first exploration for bulk tonnage gold exploration in the region occurred in the 1980s through the early 2000s after the discovery of the Fort Knox deposit in Alaska. In the Yukon, this initial exploration led to the discovery of two past-operating mines: Brewery Creek which operated from 1996 to 2002; and more recently, Dublin Gulch

(Eagle Gold Mine) which was in operation from 2019 to 2024. Following this initial period of exploration success, RIRG research was mainly focused along the western part of the TGB (e.g., Mair et al., 2000; Marsh et al., 2003; Hart et al., 2004; Hart, 2007; Kirk, 2016; Cave et al., 2019).

This study aims to document and compare intrusive phases, mineralogy and alteration at four RIRG deposits across the Yukon portion of the TGB. The deposits visited as part of this study include the past-producing Brewery Creek mine, the RC Gold project, the Steiner deposit at the past-producing Eagle Gold Mine, and the newly defined Valley deposit (Fig. 2). Brewery Creek and the RC Gold project both host more than one defined deposit. Brewery Creek consists of 11 deposits across the Reserve trend and Classic zone and the RC Gold project consists of deposits at both Blackjack and Eiger. For clarity, this paper refers to each of these projects as single global deposits in reference to comparing four deposits across the district, though details of each respective intrusive hosts and mineralization are discussed in more detail in each deposit write up.

Host rocks, mineralized veins and alteration assemblages are described in detail from key areas of these deposits using field observations, whole-rock geochemistry and petrography. Preliminary findings highlight the importance of documenting vein textures and mineralogy, vein boundaries (e.g. sharp versus diffuse), vein sinuousity, associated vein selvedge alteration, and crosscutting relationships of veins. In comparison to porphyry deposits, alteration in RIRG deposits is predominantly restricted to vein selvedges (within 0.5–5 cm of veins). This study shows that early sulphide-poor (3–5% sulphide minerals) Au-bearing quartz veins found in the core of each deposit typically have a high-temperature potassic (locally sodic) alteration assemblage compared to sulphide-rich (>10% sulphide minerals) quartz veins found near the periphery of deposits which are also commonly paragenetically later and have a low-temperature phyllic (sericitic) alteration assemblage (Sillitoe, 2010).

Regional geology

The four deposits from this project are located within the northern Cordillera in the Selwyn basin region (Fig. 2). The Selwyn basin was an arcuate embayment in the Lower Paleozoic passive margin of ancestral North America characterized by deposition of deep water, off-shelf and slope facies sediments, along the ancestral North American margin (Abbott et al., 1986; Cecile et al., 1997). Early Cambrian to Late Ordovician mafic volcanic rocks occur sporadically throughout the Selwyn basin, representing minor extension and episodic tectonic instability along an otherwise passive continental margin (Goodfellow et al., 1995; Abbott, 1997; MacNaughton et al., 2016; Cobbett et al., 2023). Passive margin sedimentation along the margin continued until the mid-Late Devonian, when subduction along the margin led to rifting in the back-arc, opening of Slide Mountain ocean, and separation of Yukon-Tanana terrane from the continent (Colpron et al., 2006; Cobbett et al., 2021). The boundary between rocks of the Laurentian margin strata and accreted remnants of Slide Mountain ocean is marked by the Jura-Cretaceous Inconnu thrust and equivalent structures (Murphy et al., 2006). Accreted geological belts and bounding structures are offset by the Cenozoic Tintina fault, a dextral strike-slip fault with 430–490 km of displacement (Fig. 1; Gabrielse et al., 2006).

The oldest rocks exposed in the Selwyn basin are the Neoproterozoic–Early Cambrian Hyland Group. The group consists of a thick succession (>3.5 km) of marine clastic and lesser carbonate rocks (Gordey and Anderson, 1993). The Hyland Group comprises the Yusezyu, upper limestone member (locally Algae) and Narchilla formations and is overlain by laterally continuous deposits of shale, chert and limestone of the lower Cambrian Gull Lake Formation,

the Cambrian to Ordovician Rabbitkettle Formation, and the Ordovician to Devonian Road River Group (Abbott, 1997; Gordey, 2013). Early Cambrian to Late Ordovician mafic volcanic rocks occur sporadically throughout the Selwyn basin, representing minor extension and episodic tectonic instability along an otherwise passive continental margin (Fig. 3; Goodfellow et al., 1995; Abbott, 1997; MacNaughton et al., 2016; Cobbett et al., 2023).

The Yusezyu Formation is the oldest unit in the Hyland Group and comprises abundant coarse-grained sandstone, pebble conglomerate ('grit') and interbedded siltstone and shale capped by a locally prominent upper limestone member (correlative with the Algae Formation in the Rackla Group; Gordey and Anderson, 1993; Cecile, 2000; Moynihan et al., 2019). The Narchilla Formation is the youngest and uppermost unit and comprises maroon, green and grey shale, slate and green quartzose siltstone (Fig. 3; Gordey and Anderson, 1993).

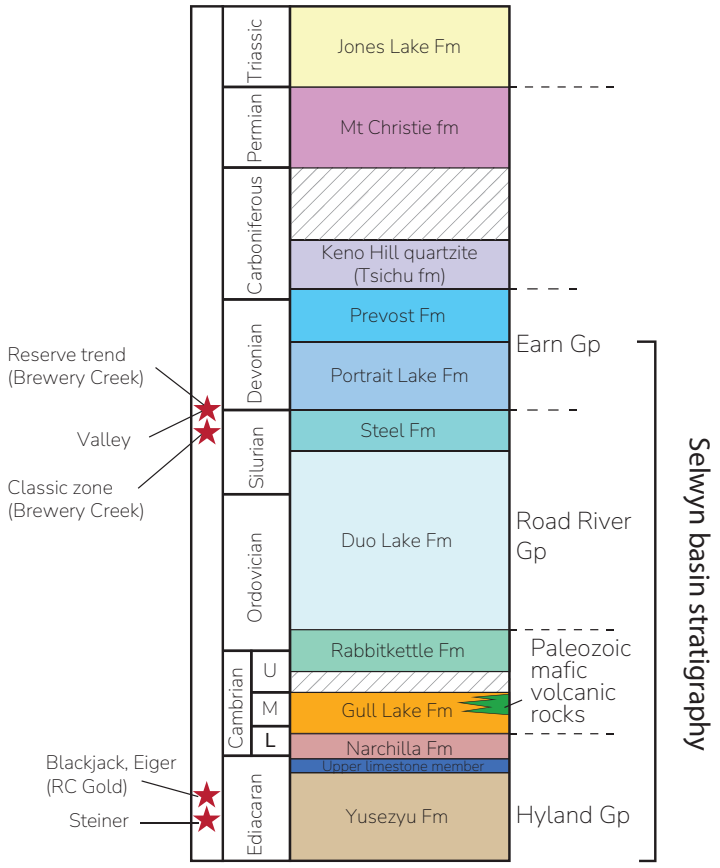

Figure 3. *Simplified stratigraphy across the Selwyn basin region with the location of each of the deposits examined in this study. Deposit locations are depicted by red stars to the left of the corresponding stratigraphy. Unconformities are omitted on this section; diagonal lines represent gap in time. Modified from Sack et al. (2018) and Roots (1997, 1998, 2003).*

The Hyland Group is overlain by the Cambrian Gull Lake Formation which is dominated by fine clastic rocks (shale, siltstone and mudstone) including local volcanic units and a basal conglomerate (Gordey and Anderson, 1993; Murphy, 1997). This is in turn overlain by thin-bedded limestone and siltstone of the Cambrian to Ordovician Rabbitkettle Formation (Gabrielse et al., 1973). Ordovician to Devonian Road River Group, which includes the Duo Lake and Steel formations, occurs above the Rabbitkettle Formation and consists of non-calcareous shale interbedded with thin-bedded, black to dark grey chert and argillaceous chert (Gabrielse et al., 1973; Cecile, 1982; Gordey and Anderson, 1993). The Devonian Earn Group predominantly consists of a lower section of chert, siltstone, and siliceous shale, and an upper section dominated by chert pebble conglomerate, chert-quartz sandstone with lesser chert, and fine-grained siliciclastic rocks (Fig. 3; Cobbett et al., 2021).

The Selwyn basin region was deformed into northwest-trending folds and thrusts in the

Late Jurassic to Early Cretaceous, as deformation propagated to the NE following accretion of allochthonous terranes (Murphy, 1997; Roots, 1997). Extensive mid-Cretaceous back-arc magmatism occurred in the back-arc region which locally overlapped with the latest phases of deformation (e.g., Jennings and Gilson, 1986), but mostly occurred after penetrative deformation had ceased. This magmatism is interpreted to be unrelated to active subduction or convergent boundaries and is instead associated with a post-collisional extensional regime following compression (Hart et al., 2004). These intrusions are predominantly felsic to intermediate in composition and display a variety of grain sizes (fine to coarse) and textures (equigranular to megacrystic). The relative modal abundance of mafic minerals in these intrusions is used as a key distinguisher and is typically denoted by the 'Hbl>Bt' (modal abundance of hornblende is greater than that of biotite) or 'Cpx=Hbl' (modal abundance of clinopyroxene is equal to that of hornblende) notation.

Tombstone gold belt, plutonic suites and metallogenic characteristics

The Tombstone gold belt represents the innermost plutonic belt in the Selwyn basin and forms a linear belt of over 100 plutons across three intrusive suites (Tungsten, Mayo and Tombstone) that are recognized by their distribution, composition and metallogenic signature (Fig. 2; Hart et al., 2004). The eastern Tungsten plutonic suite (98–95 Ma) comprises small, typically round plugs and plutons of felsic, peraluminous, equigranular to K-feldspar porphyritic (locally megacrystic), fine to coarse-grained biotite monzogranite and leucogranite (Rasmussen, 2013). Additional fine-grained equigranular leucocratic muscovite ± biotite, garnet and/or tourmaline-bearing phases are also commonly observed (Rasmussen, 2013). Tungsten skarns, sheeted quartz ± tourmaline veins and associated greisen may be mineralized with scheelite or auriferous pyrite ± arsenopyrite (Rasmussen, 2013). This study does not include any Tungsten suite intrusions.

The central Mayo plutonic suite (98–93 Ma) comprises small, massive to foliated, sub-alkalic, metaluminous to peraluminous, reduced to slightly oxidized (titanite ± magnetite-bearing), homogenous to composite plutons (Rasmussen, 2013). These intrusions vary from fine to coarse-grained, equigranular to porphyritic to coarsely megacrystic, quartz-monzonite, monzodiorite, monzogranite and granodiorite (Rasmussen, 2013). Typically, intrusions have modal abundances of biotite>hornblende, although hornblende>biotite in quartz-monzonite to monzodiorite is also locally observed (Rasmussen, 2013). Intrusions are typically cut by aplitic to leucocratic granite dikes, graphitic quartz-tourmaline veins, tourmaline-infilled vugs and auriferous sheeted veins (Rasmussen, 2013). The mineralizing intrusive rocks at the Blackjack and Eiger (RC Gold), Steiner and Valley deposits are part of the Mayo suite.

The central to western Tombstone plutonic suite (94–90 Ma) comprises scattered intrusions or clusters of round, commonly concentrically zoned alkalic, variably fractionated, slightly to moderately oxidized, composite plutons (Hart et al., 2004; Rasmussen, 2013). Medium to coarse-grained, K-feldspar syenites are the most common intrusions in the western Selwyn basin. In the eastern Selwyn basin, the Tombstone suite is represented by sub-alkaline, fine to coarse-grained quartz-monzonite and monzogranite with modal minerals hornblende>biotite and hornblende>clinopyroxene (Rasmussen, 2013). The mineralizing intrusions at the Brewery Creek deposits (Reserve trend and Classic zone) are part of the Tombstone suite.

Reduced intrusion-related gold systems (RIRGS)

This study focuses on the intrusion-hosted deposit examples within the broader mineralizing

RIRG system (RIRGS). The general model for RIRG deposit mineralization is summarized from Marsh et al. (2003). In this model, magma is emplaced within an extensional environment at 5–7 km depth (~2 kbar). Initial cooling of the magma forms a carapace along the top and margins of the intrusion while the remaining melt continues to fractionate. Continued extension results in sheeted fractures in the brittle carapace thereby reducing overlying lithostatic pressure resulting in fluid exsolution and initial ore fluid formation. Fractures are typically filled with 0.5–5 cm wide auriferous, low-sulphide (<5%) quartz veins in sheeted arrays with a relatively reduced ore mineral assemblage (arsenopyrite, pyrrhotite, pyrite). Continued reduction in pressure results in fluid unmixing into high and low-salinity CO_2–rich fluids. Sulphide ± gold-bearing fluids continue to fill sheeted fractures at higher temperatures (350–300˚C). As the system cools, brittle faults develop and lower temperature (300–250˚C) silver-rich fluids crosscut or occupy previous vein structures. This often creates a predictable zoning pattern within and outboard of the causative intrusion (Fig. 4).

While this study focuses on one aspect of these mineralizing systems (intrusion-hosted, Au-bearing quartz-sulphide veins), these systems are associated with other styles of mineralization. For example, gold ± tungsten skarns and replacement-style mineralization (e.g., Mactung) associated with calcareous host rocks, late and or peripheral (Au-Sb-As)-Ag-Pb-Zn veins, as well as sediment-hosted intrusion-related gold deposits which may not have a causative intrusion identified (e.g., AurMac; Fig. 5).

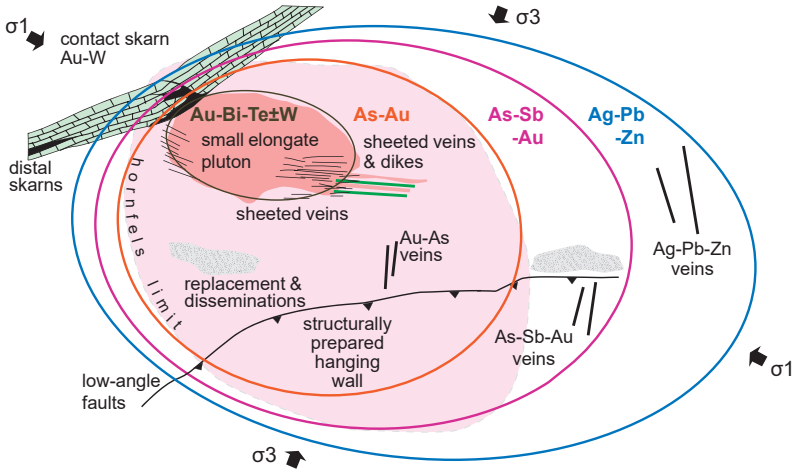

Figure 4. *Plan-view model of interpreted reduced intrusion-related gold system zoning from this study highlighting mineralization styles and predictable geochemical zoning patterns outboard of the intrusion. σ1 is the direction of the largest compressive stress, σ3 is the direction of least stress. Modified from Hart et al. (2002). Au = gold, W = tungsten, Bi = bismuth, Te = tellurium, As = arsenic, Sb = antimony, Ag = silver, Pb = lead, Zn = zinc.*

Methods

Three to five days were spent logging drill core at each of the four deposits included in this study; a total of 11 holes and approximately 3500 m. Drill core logging focused on representative 'high-grade' mineralization, 'low-grade' mineralization, and non-mineralized intervals at each deposit. Field observations were made regarding lithology, vein morphology and mineralogy, as well as associated alteration. Non-mineralized intervals of all major host intrusions with the least alteration possible were selected as representative samples for whole-rock analyses from each deposit. The exception being samples chosen from the Brewery Creek deposits which are all weakly to moderately altered. This alteration likely

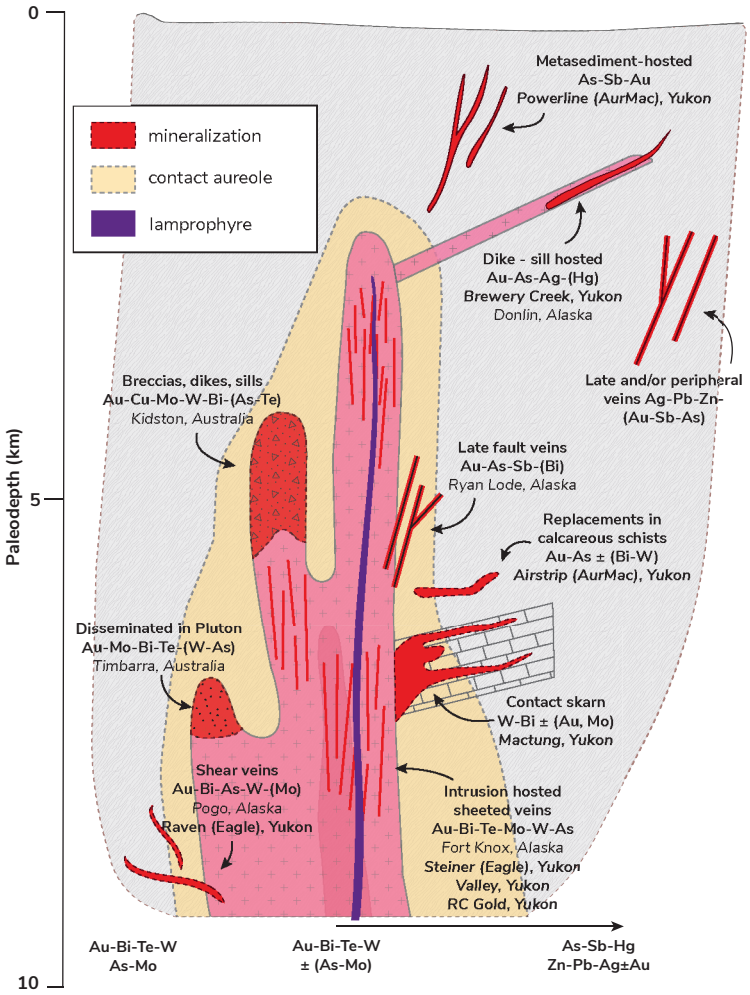

Figure 5. *Diagram illustrating the distribution and relationship of zoning for reduced intrusion-related gold systems and the interpreted distribution of deposit types with examples. Modified from Lang et al. (2000).*

skews whole-rock trends of these samples to be more alkalic. Additional information can be found in Appendices A and B.

Modal calculations for QAP ternary diagrams and rock name classifications were made using petrography and ImageJ, a java-based image processing software (https://imagej.net/ij/). Grain size nomenclature uses the following parameters: fine grained (<1 mm), medium grained (≥1 to <5 mm), coarse grained (≥5 to <20 mm) and very coarse grained (≥20 mm). The mineralogical naming convention in this study uses '>' (greater than), '<' (less than) and '–' (equal to) to highlight the relative modal abundance of mafic minerals when modifying a given rock name. Mineral abbreviations follow the Whitney and Evans (2010) convention. Magnetic susceptibility measurements reported were collected over broad intervals in drill core producing an average value from five measurements. Additional magnetic susceptibility measurements were systematically taken of each sample during sample preparation after field work was completed.

A total of 137 representative samples (135 half-cut NQ2 and HQ drill core, and 2 open-pit samples) were collected across the four properties: Brewery Creek (Reserve trend and Classic zone), RC Gold (Blackjack and Eiger), Steiner and Valley. From the sample selection, 24 samples were sent for whole-rock complete characterization (Appendices B and C), and 64 polished thin sections were made of all intrusive phases including whole-rock samples, as well

as of representative veins, mineralization and alteration types.

Whole-rock samples were pre-cut to ≥250 g samples and oxidation and veins were removed prior to submission to ALS Laboratories (ALS) in Vancouver, British Columbia (BC). Whole-rock complete characterization was carried out using CCP-PKG03, which analyzes major elements by fusion decomposition followed by x-ray fluorescence, total carbon by C-IR07 and total sulphur by S-IR08, trace elements by lithium borate fusion followed by acid dissolution and inductively coupled plasma atomic emission spectroscopy (ICP-AES), volatiles by aqua-regia digestion and inductively coupled plasma mass spectrometry (ICP-MS), and base metals by four-acid digestion followed by ICP-AES.

Thin section samples were pre-cut into billets prior to shipment to Vancouver Petrographics in Langley, BC. All offcut billets and seven core samples were stained with sodium cobaltinitrate to identify the presence of K-feldspar (Bailey and Stevens, 1960) to use in QAP classification and alteration characterization.

Brewery Creek

Five days were spent on site logging three representative holes and selectively sampling four additional holes and two pits at the former Brewery Creek mine. Logging was focused on several targets along the Reserve trend (Kokanee, Bohemian, Schooner, Sleeman, Moosehead, and West Big Rock) and at the Classic zone (Fig. 6). Drill core was predominantly from 2011 and 2012 drill campaigns and one 1998 drill hole was sampled from the Kokanee deposit. Brewery Creek was in operation between 1996 and 2002 and produced 280 000 oz of Au from seven near-surface oxide deposits (Cook et al., 2022). The current global resource consists of 11 deposits across the Reserve trend and Classic zone totaling 2.1 Moz Au (1 140 000 oz Au Measured and Indicated; 1 020 000 Inferred; Cook et al., 2022). The Brewery Creek deposits are the only Tombstone suite-associated deposits in this study. The Reserve trend deposits are also the most oxidized of all the examples in this study. Fifty-one representative samples were taken; nine were sent for whole-rock analysis and fifteen polished thin sections were made.

Property scale geology

Brewery Creek is located in east central Yukon, 55 km east of Dawson City (Fig. 1). The deposits are hosted by Paleozoic sedimentary rocks of the Earn and Road River groups where they are intruded by Tombstone suite intrusions (Figs. 3 and 6). Sill emplacement is primarily controlled by a graphitic argillite at the contact of the Earn and Road River groups (Cook et al., 2022). The sedimentary rocks have been deformed by a series of folds and thrusts, which form a NNE-trending arch of thrust sheets resulting in upright to steeply inclined, open to tight, variably NE, E and NW-trending folds (Lindsay, 2006). The Reserve trend is hosted within a series of NW and E trending quartz-monzonite, monzonite and hornblende gabbro sills that vary in thickness from <1 m to >1 km and are exposed over 12 km (Lindsay, 2006). The intrusions crosscut the thrust faults and folds but are offset by variably oriented strike-slip faults (Fig. 6; Lindsay, 2006). At the Classic zone, the deposit is hosted within an alkali syenite pluton with NW-trending gold-bearing sheeted veins parallel to the NW-trending Classic fault (Lindsay, 2006).

Intrusive rock descriptions and field relationships

There are two main intrusive host lithological units at Brewery Creek. Along the Reserve trend, the main lithology is a fine to medium-grained, porphyritic hornblende biotite quartz-monzonite

to monzonite. At the Classic zone, the main intrusion is a medium to coarse-grained to locally very coarse-grained and crowded alkali (K) feldspar syenite. The intrusions at Brewery Creek are metaluminous, magnesian, alkalic (Classic zone) to alkali-calcic (Reserve trend), and silica-saturated, whereas the intrusions at the Classic zone are close to silica-undersaturated (Fig. 7). Though care was taken to obtain the least altered representative samples from drill core, petrographic and alteration box plot indices show weak to moderate alteration within all samples which inherently skew whole rock data for these samples to slightly more alkalic compositions.

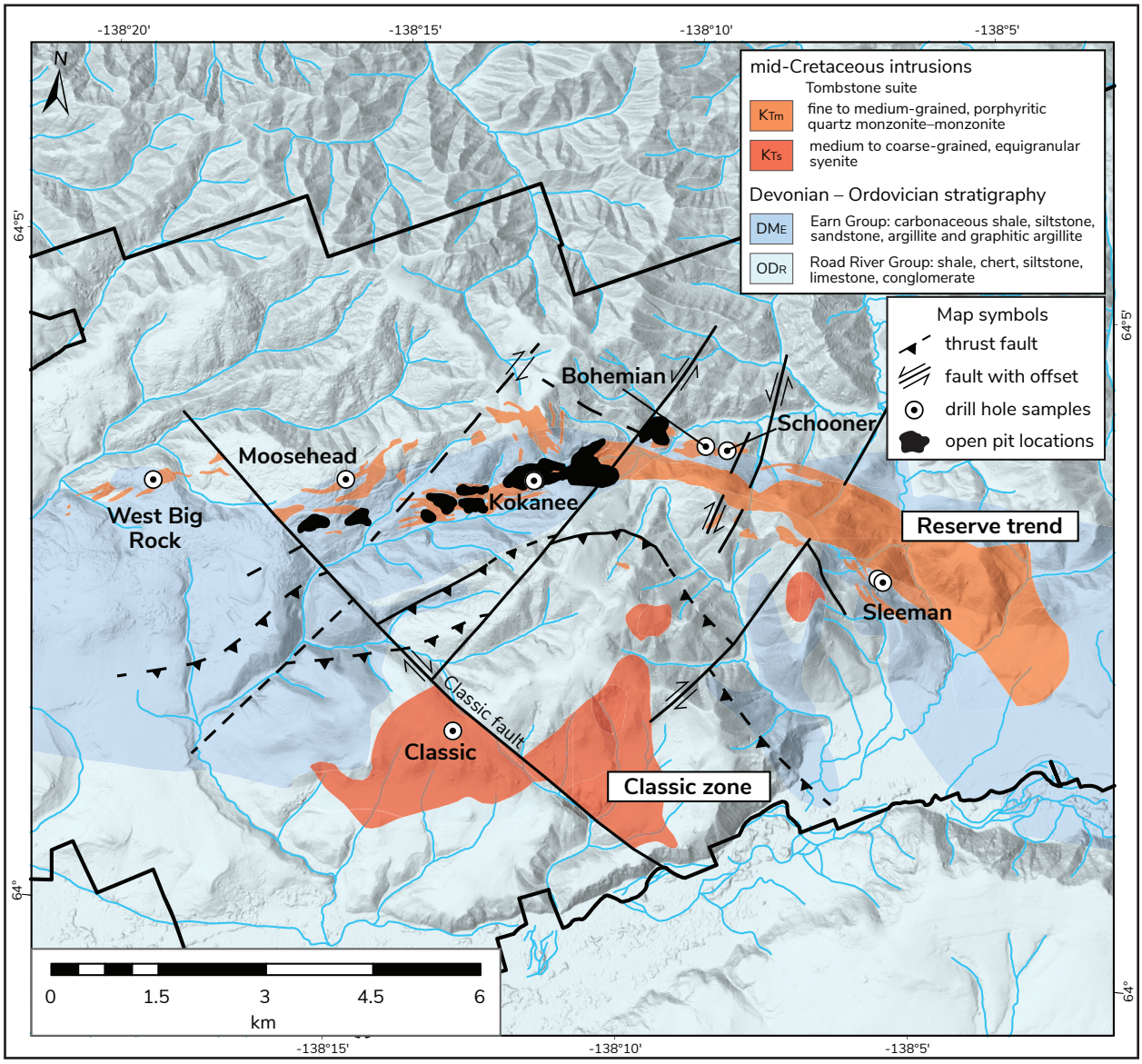

Figure 6. *Simplified Brewery Creek property geology. Property-scale intrusions and simplified structural data are from Lindsay (2006), bedrock geology is sourced from Yukon Geological Survey (2024), 1:250 000 scale to correlate with Figure 3. Black polygons are past open pit locations from when the mine was in operation. White circles represent collars from holes that were logged and selectively sampled.*

Fine to medium-grained porphyritic hornblende biotite quartz-monzonite

The main intrusion along the Reserve trend is a grey to medium grey, fine to medium-grained porphyritic hornblende>biotite quartz-monzonite. The groundmass is fine to medium

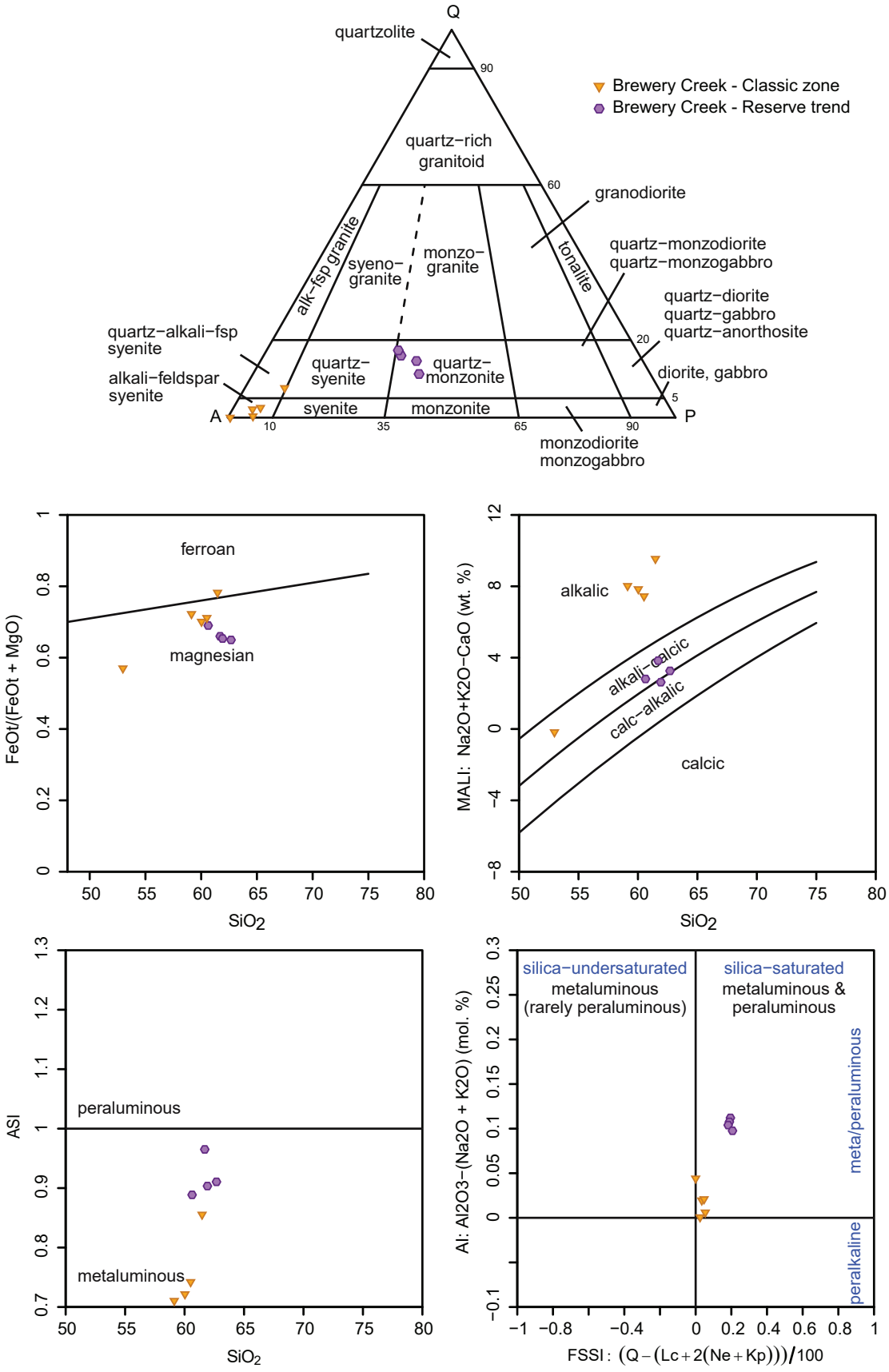

Figure 7. *QAP ternary diagram of Brewery Creek intrusive rocks and Frost and Frost (2008) classification of representative whole rock samples.*

grained and comprises K-feldspar, quartz and plagioclase (sub-mm to 2 mm) with 30 to 40% phenocrysts of subhedral to anhedral alkali (K) feldspar and plagioclase (2 mm to 1 cm long), biotite, hornblende, pyroxene and minor quartz (2–6 mm; Fig. 8a,b). Modal compositions vary slightly in the deposits sampled across the Reserve trend however the dominant rock forming minerals are approximately alkali (K) feldspar (20–30%), plagioclase (20–30%), hornblende (15–20%), pyroxene (10%), biotite (5–10%) and quartz (5–10%). Average magnetic susceptibility is 0.371×10^{-3} SI units (N=10).

In thin section plagioclase is commonly euhedral and displays compositional zoning and polysynthetic twinning. Plagioclase crystals are typically 1 to 6 mm across and locally form glomerocrysts up to 12.5 mm across. Plagioclase also locally displays antiperthitic textures (Fig. 9). Less than 5% of phenocrysts comprise K-feldspar. Quartz phenocrysts are rare and typically anhedral and embayed (Fig. 9e). Most feldspars are weakly to moderately sericitized, with stronger alteration present in cores than in the rims (Fig. 9).

Mafic minerals present include hornblende, biotite and pyroxene, all of which display moderate to strong chlorite alteration across all representative samples taken. Hornblende is the most abundant mafic mineral and is often moderately to completely replaced by orange-brown secondary biotite (Fig. 9). Most primary biotite grains are shredded, light to medium orange-brown and have weak to moderate patchy chlorite alteration. Pyroxenes are colourless, typically euhedral, ranging from 0.5 to 2.5 mm in diameter, and are often observed grown together as glomerocrysts with other mafic minerals (Fig. 9). Minor disseminated sulphides (dominantly arsenopyrite and pyrite) are predominantly observed replacing or intergrown with mafic minerals.

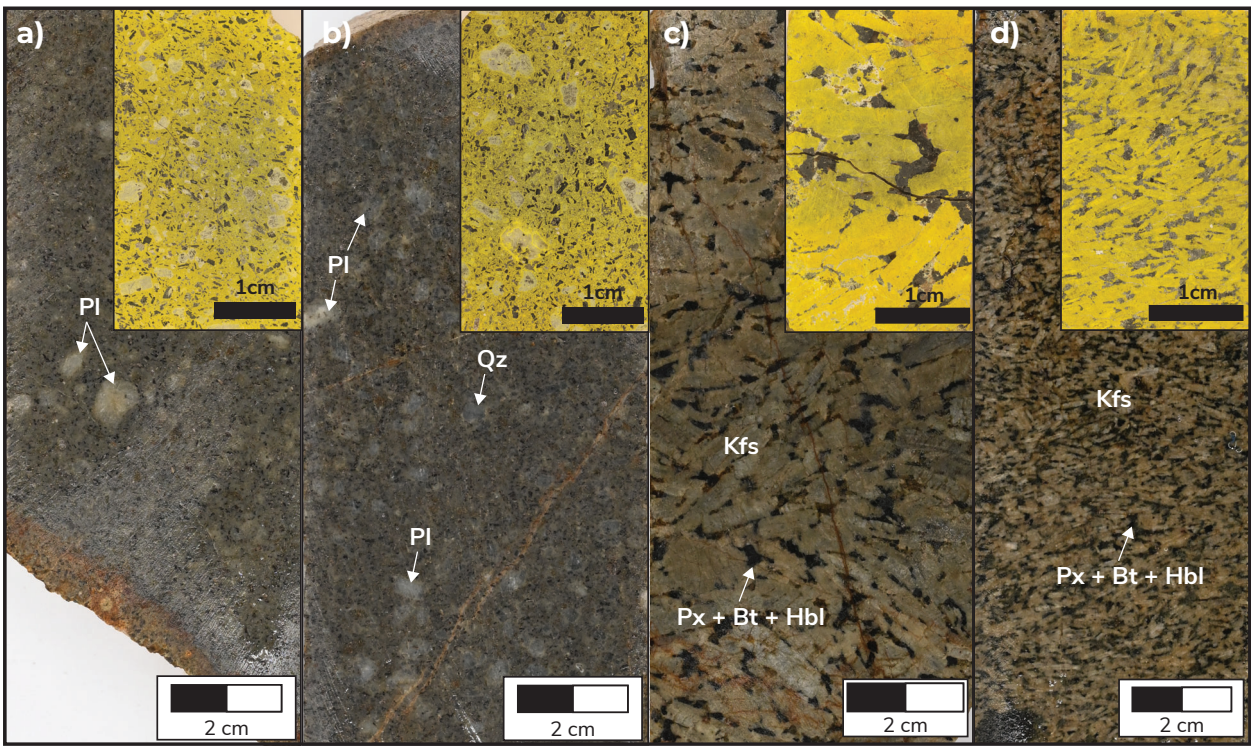

Figure 8. *Drill core samples from Brewery Creek Reserve trend (a) BC11-200_51.7m, (b) DD98-109_59.3m and Classic zone (c) BC11-373_182.2m, (d) BC11-373_231.9m. Inset figures are billet offcuts from corresponding thin sections cut from the sample. Samples (a) and (b) are fine to medium-grained porphyritic hornblende biotite quartz monzonite. Samples (c) and (d) are medium (d) to coarse (c) grained equigranular pyroxene biotite hornblende alkali syenite. Bt=biotite, Kfs = K-feldspar, Pl = plagioclase, Px = pyroxene, Qz = quartz, Hbl = hornblende.*

Medium to coarse-grained, locally very coarse and crowded equigranular biotite hornblende pyroxene K-feldspar syenite

The host intrusion at the Classic zone is a cream-grey to grey-brown, medium-grained to very coarse grained, equigranular biotite hornblende pyroxene K-feldspar syenite (Fig. 8c,d). Phenocrysts of felted euhedral alkali (K) feldspar vary in length from 1 to 4 mm, with locally very coarse and crowded K-feldspar phenocrysts 0.5 to 2 cm long. Modal compositions are approximately alkali (K) feldspar (60%), pyroxene (18%), hornblende (10%), biotite (5– 10%), quartz (5–10%) and disseminated arsenopyrite (1-2%) and minor pyrite in the groundmass. The average magnetic susceptibility is 0.351 × 10^{-3} SI units (N=8).

Felsic minerals (dominantly K-feldspar, minor plagioclase, trace quartz), comprise 60 to 70% of the total rock and mafic minerals (pyroxene, biotite and lesser hornblende) comprise ~30 to 40%. K-feldspar laths are weakly to moderately aligned, 5 to 12.5 mm across with simple twinning and strong perthitic textures in all grains (Fig. 9). Very minor euhedral to subhedral plagioclase is observed along K-feldspar boundaries. All feldspars are weakly to moderately sericite altered. K-feldspar phenocrysts commonly contain minor pyroxene inclusions.

Mafic minerals are pyroxene, biotite and lesser hornblende. Pyroxene is light to medium green and observed as single grains or as glomerocrysts with orange-brown biotite and minor titanite (Fig. 9). Biotite and hornblende occur as subhedral to anhedral masses 1 to 4 mm in length, between K-feldspar laths. Minor euhedral titanite is observed throughout and associated with mafic minerals. Arsenopyrite is disseminated in trace amounts and is found near titanite (Fig. 11).

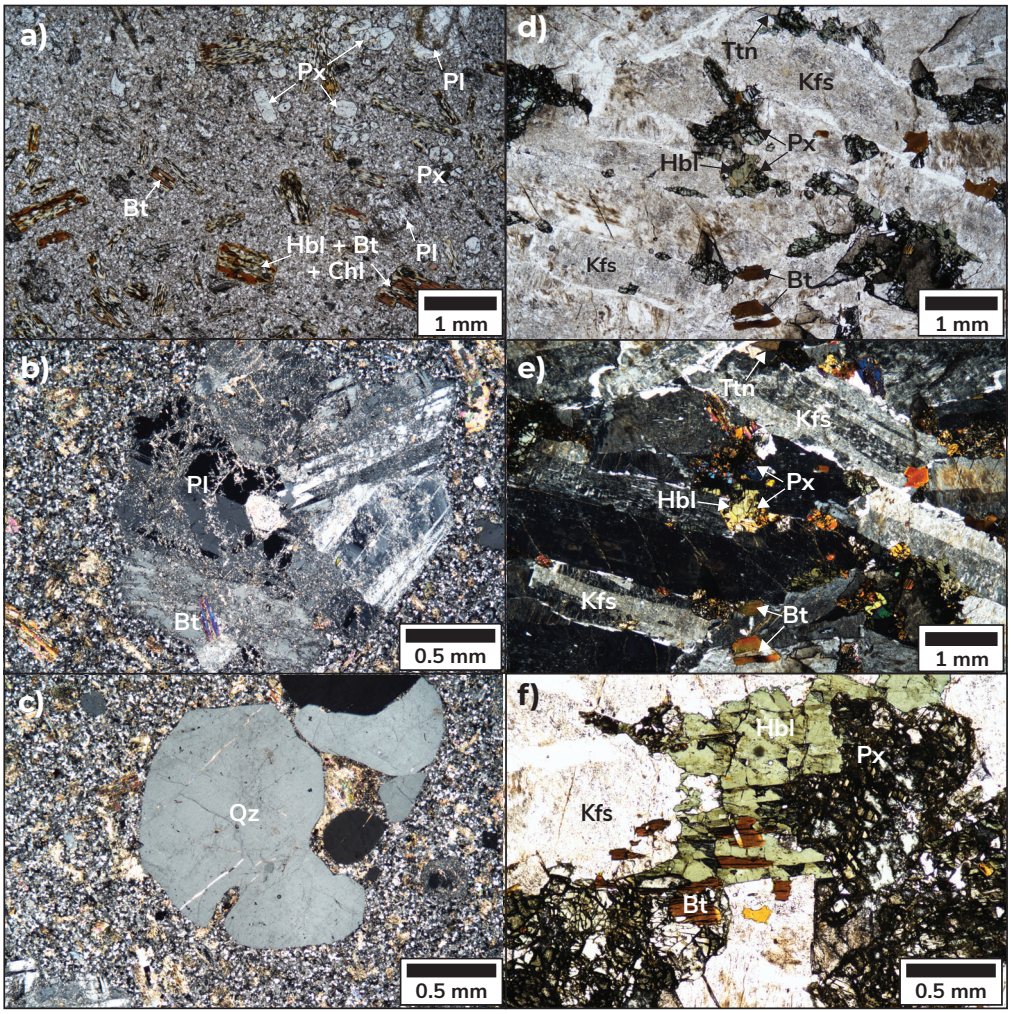

Figure 9. *Plane polarized (a, c, e) and cross polarized (b, d, f) photomicrographs of host intrusions at Brewery Creek. Samples on the left (a) 24PS56-1, (c) BC12-478_94.5m and (e) BC12-478-94.5m are from quartz monzonite samples in the Reserve trend. Samples on the right (b) BC11-373_231.1m, (d) BC11-373_231.1m and (f) BC11-373_231.1m are from the Classic zone syenite. Ttn = titanite, Chl = chlorite.*

Veins, mineralization and alteration

Gold at the Brewery Creek deposits occurs as fracture and fault-controlled disseminations and in quartz-sulphide veins within intrusions as well as in the surrounding sedimentary rocks (Lindsay, 2006). The veins at the Reserve trend have two distinct orientations, east and northeast, and appear to be bound at depth by a moderately dipping, east-striking normal fault (Lindsay, 2006). Prior studies have identified four paragenetic stages related to mineralization: pre-Tombstone suite intrusions, syn-Tombstone suite intrusions, post-Tombstone suite intrusions (Au-bearing) and lastly Au-remobilization due to weathering (Lindsay, 2006). Mineralization is typically characterized by a Au-As-Sb ± Ag-Pb metal association signature. Gold is refractory and dominantly associated with, and hosted in, arsenopyrite and arsenian pyrite (Lindsay, 2006).

In the Reserve trend deposits, the dominant vein style is quartz-carbonate-arsenopyrite (± pyrite, hematite, stibnite) veins which are steeply south-dipping and contain 10 to 80% arsenopyrite (Fig. 10). Sulphide-dominant veins containing arsenopyrite ± pyrite are secondary and are often oxidized to limonite-jarosite and scorodite in vein selvedges (Fig. 10). Quartz-sulphide cemented polymictic breccias, fault-controlled disseminated sulphides, vuggy quartz

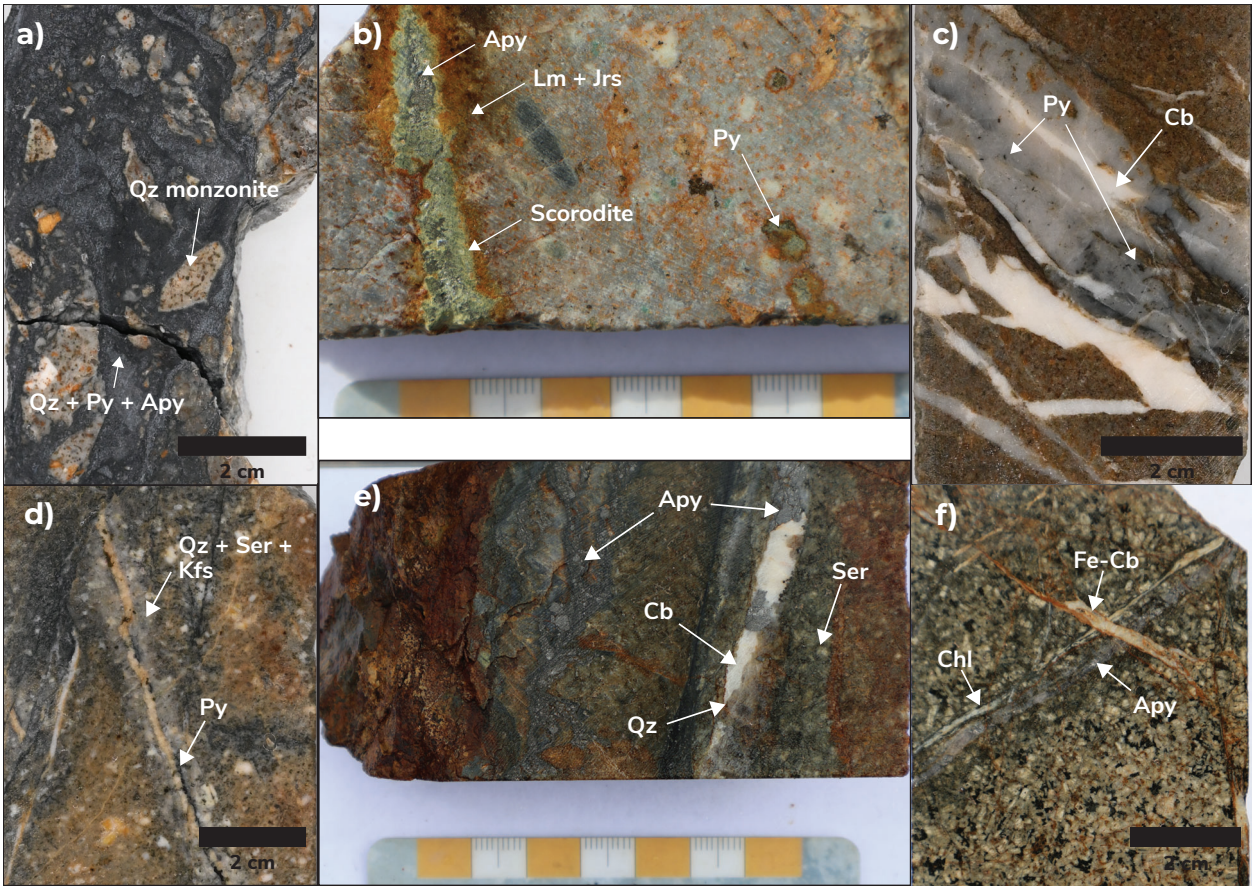

Figure 10. *Examples of mineralized intervals at Brewery Creek. Samples (a) to (d) are from the Reserve trend, samples (e) and (f) are from the Classic zone.* ***(a)*** *BC12-466_40m: quartz-sulphide cemented breccia in quartz monzonite.* ***(b)*** *BC11-175_30.3m: massive arsenopyrite vein with scorodite and Lm-Jrs in vein selvedge in quartz monzonite.* ***(c)*** *BC12-478_142.6m: banded quartz-pyrite-arsenopyrite vein with late carbonate veins.* ***(d)*** *BC11-175_60.4m: pyrite-carbonate vein with a Qz-Ser-Kfs halo.* ***(e)*** *BC11-373_104.1m and* ***(f)*** *BC11-373_136.9m display examples of arsenopyrite veins and sulphide breccias at the Classic zone with pervasive silica and sericite alteration in wall rock (e) and late Fe-carbonate veins (f). Ser = sericite, Apy = arsenopyrite, Py = pyrite, Cb = carbonate, Fe-Cb = iron carbonate, Lm = limonite, Jrs = jarosite.*

veins with cockscomb textures and sheeted sulphide-poor quartz veins with pyrite and arsenopyrite were also observed (Fig. 10). In thin section, arsenopyrite, pyrite and very minor chalcopyrite are disseminated throughout quartz-carbonate veins and within surrounding wall rock (Fig. 11). Sulphides are often spatially associated with titanite.

In the Classic zone deposit, millimetre-scale sheeted quartz-arsenopyrite-carbonate veins average 1 to 5 veins/m in assay-identified Au mineralized zones (Fig. 10). Quartz-arsenopyrite veins are locally offset by oxidized fractures and crosscut by quartz-iron carbonate-pyrite veins. Lower angle Fe-carbonate veins locally follow the same vein structure. Rare, banded quartz-sulphide veins and clay-matrix-supported, well-milled, poorly sorted and unconsolidated fault breccias with disseminated sulphides were also observed. In addition to vein density, breccias and disseminated sulphide, increased grade corresponds to late faulting (Fig. 10). Disseminated (≤1%) arsenopyrite and pyrite within the groundmass of the host intrusion is common within mineralized intervals.

Alteration and oxidation at the Brewery Creek deposits is commonly fault-controlled. Oxidation was observed to a depth of at least 200 m in drill core. Strong pervasive, texturally destructive silica, sericite ± carbonate alteration is common adjacent to faulting and extends several metres into surrounding host rock. Fracture-controlled to disseminated Fe-oxides (limonite, jarosite) often overprint altered intervals. Where observed in thin section, alteration in vein selvedges is characterized by K-feldspar, biotite, minor quartz and carbonate (Fig. 11)

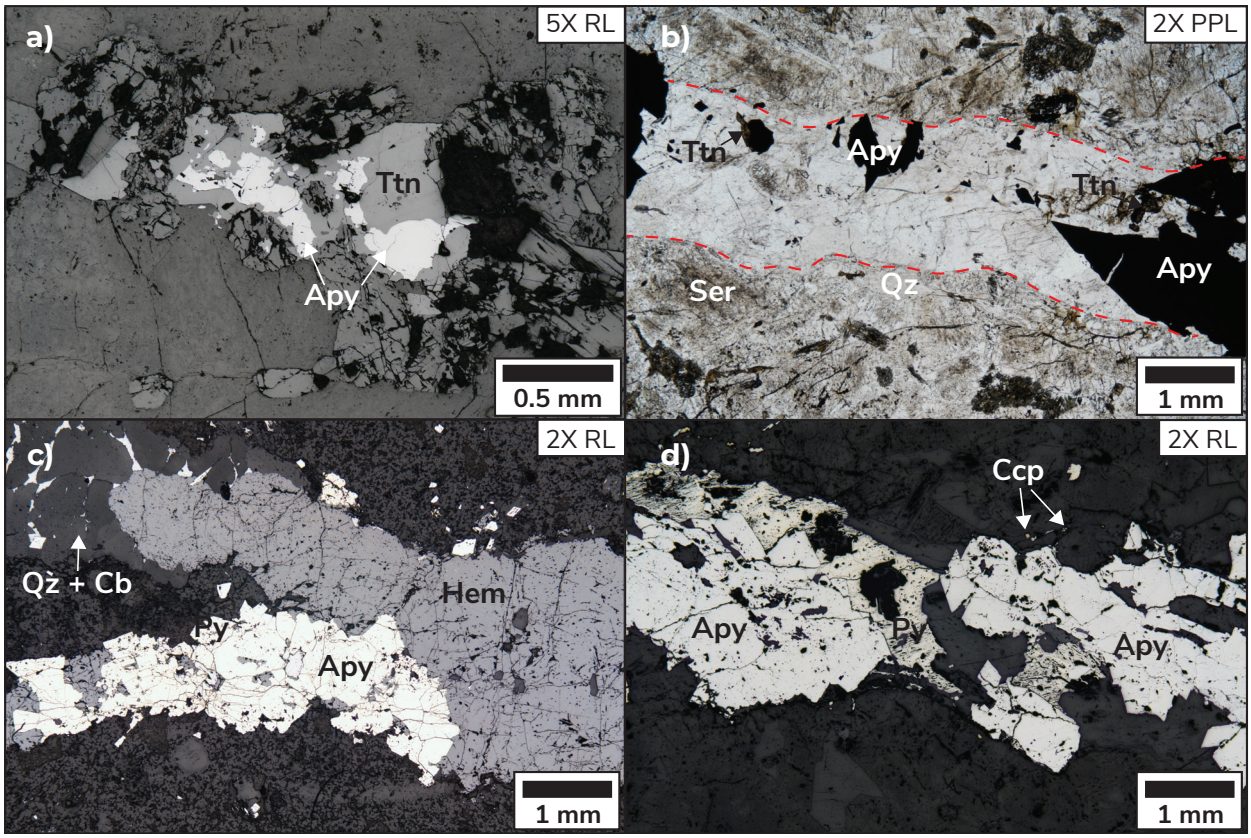

Figure 11. *Reflected and plane polarized light photomicrographs of quartz sulphide veins at the Classic zone. Titanite and arsenopyrite are often commonly spatially related in sulphide veins (a) BC11-373_231.1m, (b) BC11-373_132.8m. Samples (c) BC11-373_37.1m and (d) BC11-373_132.8m displays massive sulphide vein where arsenopyrite and pyrite are the dominant sulphides. Sample (c) displays hematite veining and quartz-sulphide veins. Hematite is red-grey in hand sample and thin section. Ccp = chalcopyrite, Hem = hematite, PPL = plane polarized light, RL = reflected light.*

RC Gold project: Blackjack and Eiger deposits

Four days were spent on site logging two representative holes from the RC Gold project's Blackjack and Eiger deposits: one hole from 2023 drilling (DDRCCC-23-041) and one hole from 2021 drilling (DDRCCC-21-009; Fig. 12). The Blackjack and Eiger deposits contain the current combined inferred mineral resource estimate at the RC Gold project (1.34M oz global resource; Simpson, 2023). Twenty-two representative samples were taken; eight were sent for whole-rock analysis and seventeen polished thin sections were made.

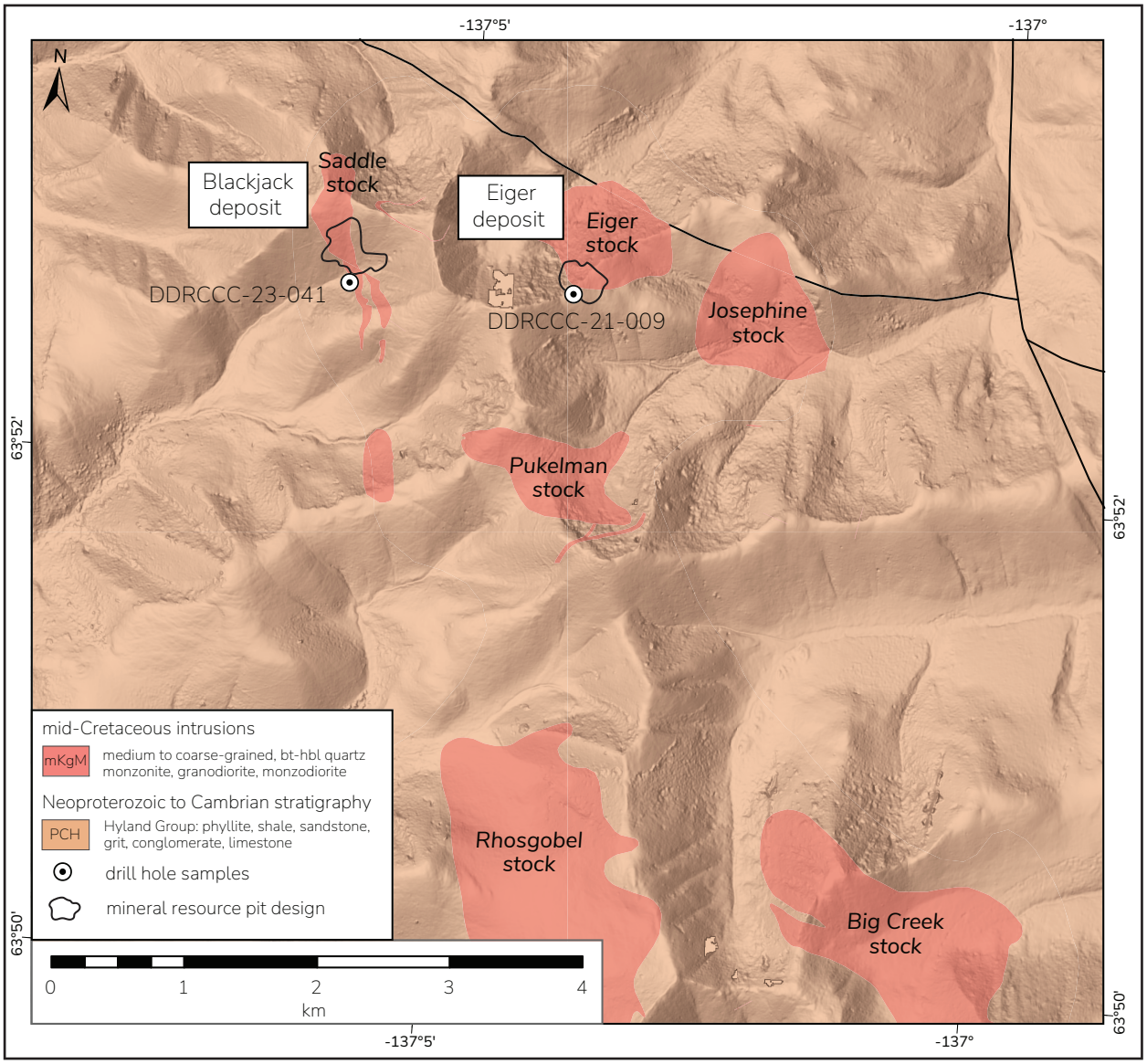

Figure 12. *Simplified RC Gold property geology. Property-scale intrusions and simplified structural data are from pers comms with Sitka Gold Corp., bedrock geology is 1:250 000 scale to correlate with Figure 3. White circles represent collars from holes that were logged and selectively sampled.*

Property scale geology

The RC Gold project is located in central Yukon, 120 km southeast of Dawson City (Fig. 1). The deposits are hosted by mid-Cretaceous intrusions within Neoproterozoic–Early Cambrian Hyland Group metasedimentary rocks (Fig. 3; Murphy, 1997; Marsh et al., 2003). The property

has at least six mid-Cretaceous intrusions with surface exposures ranging from 0.2 to 3.5 km^2 and compositions ranging from diorite (Eiger), granodiorite (Josephine, Big Creek) to quartz-monzonite (Saddle [Blackjack], Pukelman, Rhosgobel; Fig. 12; Marsh et al., 2011).The intrusions at Blackjack and Eiger are metaluminous to weakly peraluminous, magnesian, alkalic to calc-alkalic and are all silica-saturated (Fig. 13).

Intrusive rock descriptions and field relationships

At Blackjack, the main host to the deposit is a mesocratic, medium to coarse-grained K-feldspar porphyritic to locally megacrystic, biotite hornblende quartz-monzonite (Figs. 13 and 14a). Locally on a metre-scale, quartz-monzonite gradationally transitions to a medium-grained equigranular to K-feldspar porphyritic biotite-hornblende quartz-monzonite (Fig. 14b). Both of these lithological units are intruded by centimetre to metre scale fine to medium-grained K-feldspar porphyritic biotite-hornblende quartz-monzonite dikes (Fig. 14c). The orientation of the main intrusion at this deposit is elongate north-south and is often interfingered on a metre-scale with strongly hornfelsed metasedimentary rocks (dominantly biotite schist).

At Eiger, the main intrusion is a dark grey, fine to medium-grained, plagioclase porphyritic to equigranular, biotite quartz-diorite to monzodiorite (Fig. 14d). Several dikes are found throughout the drill core, which vary from dark grey to black, fine-grained feldspar and quartz porphyritic monzonite to white-cream, fine-grained aplites and medium-grained feldspar porphyritic granitic dikes.

Medium to coarse-grained K-feldspar porphyritic biotite-hornblende quartz-monzonite

The main host at Blackjack is a medium to coarse-grained, porphyritic K-feldspar, biotite-hornblende quartz-monzonite (Fig. 14a). Locally this unit is megacrystic (phenocrysts >2 cm). The groundmass is typically medium to coarse-grained, comprising plagioclase, quartz and mafic minerals that are intergrown with K-feldspar. K-feldspar phenocrysts (~5% of rock) are variable, from 0.2 to 4 cm long, often zoned, with inclusions of biotite along growth zones (Fig. 14a). Modal compositions are approximately plagioclase (30%), K-feldspar (15%), quartz (20%), biotite (25%), hornblende (10%) and disseminated sulphides (1–2%; pyrrhotite, pyrite). The average magnetic susceptibility is 0.395×10^{-3} SI units (N=2).

In thin section, phenocrysts of K-feldspar are euhedral to subhedral with inclusions of subhedral plagioclase, quartz, biotite and hornblende. Quartz is anhedral and is often intergrown with feldspar. Plagioclase makes up most of the groundmass, and zoning and polysynthetic twinning is common. Weak to moderate saussuritization is typically restricted to the inner core of plagioclase crystals (Fig. 15). Hornblende and biotite are present in equal amounts. Hornblende is 0.5 to 8 mm across, euhedral-subhedral, light to medium green and locally brown, often twinned and occurring as glomerocrysts, with inclusions of quartz, feldspar and accessory minerals. Biotite is 0.6 to 3.1 mm across, light to medium brown, euhedral to subhedral. Weak to moderate pervasive chlorite alteration of hornblende and lesser biotite is common. Trace disseminated sulphides are present and typically replace biotite or hornblende though are locally found within in the groundmass. Sulphides are dominantly pyrite and lesser pyrrhotite.

Medium-grained equigranular-porphyritic biotite-hornblende quartz-monzonite

Several less volumetrically significant intrusions were observed as dikes at Blackjack. These

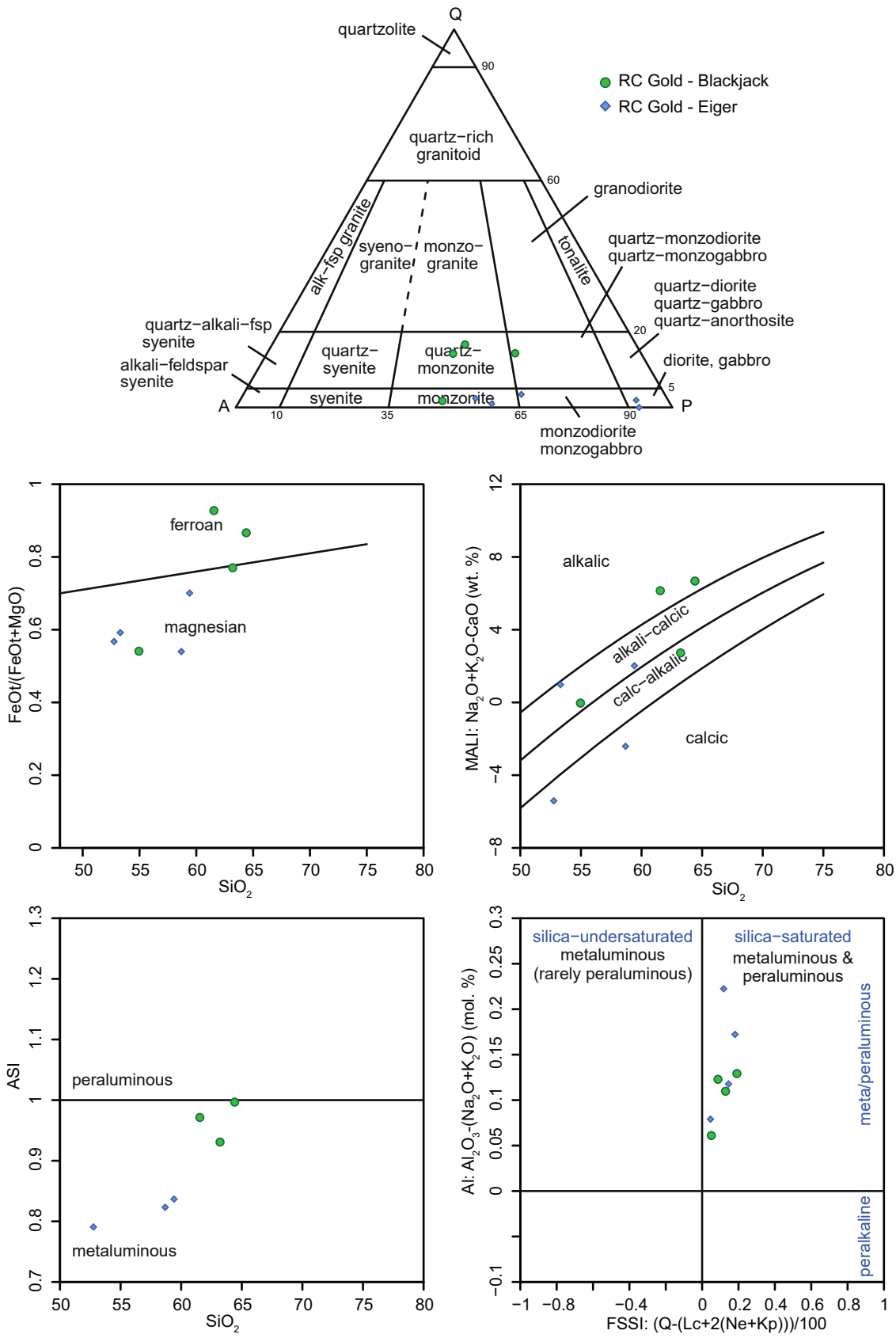

Figure 13. *QAP ternary diagram of Blackjack and Eiger intrusive rocks, and Frost and Frost (2008) classification of representative whole rock samples. Several samples on the ASI vs SiO_2 plot below the cutoff of 0.7 ASI (alumina saturation index).*

dikes are light grey, medium-grained equigranular to K-feldspar porphyritic biotite-hornblende quartz-monzonite (Fig. 14b). Phenocrysts of K-feldspar range from sub-mm up to 5 mm across with 2% ranging up to 1 cm. Modal compositions are approximately plagioclase (30%), quartz (20%), K-feldspar (20%), biotite (10%), hornblende (10%), with disseminated sulphides comprising pyrite (5%), arsenopyrite (2%), and minor pyrrhotite (<1%). Dikes range from 10 to 15 cm wide and are up to several metres wide in drill core. Smaller dikes display chilled margins inwards over a centimetre-scale, while larger dike intervals have diffuse contacts. Magnetic susceptibility averages 1.58×10^{-3} SI units (N=1).

In thin section there are equal amounts of plagioclase and K-feldspar in the groundmass; zoning and polysynthetic twinning are common in plagioclase. K-feldspar appears to be preferentially sericite altered, with some plagioclase displaying moderate saussuritization. Biotite is euhedral to subhedral, often shredded with weak to moderate patchy to pervasive chlorite alteration. Biotite after hornblende is common and it is also intergrown with trace titanite (<1%). Hornblende is green to brown with partial secondary biotite replacement. Hornblende commonly contains inclusions of quartz and feldspar. Sulphides (pyrite, lesser pyrrhotite) represent ~5% of the rock and predominantly replace mafic minerals.

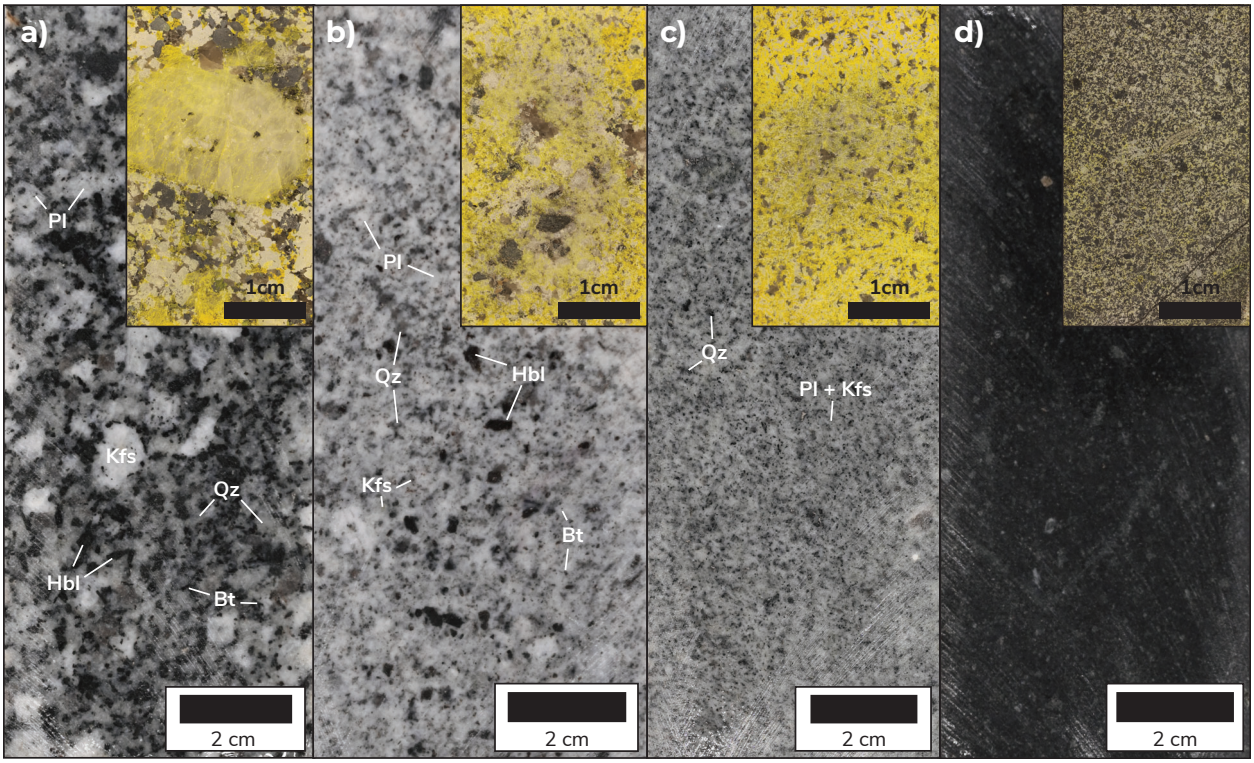

Figure 14. (a) *Medium to coarse-grained porphyritic K-feldspar biotite hornblende quartz monzonite;* ***(b)*** *medium-grained equigranular to porphyritic biotite hornblende quartz monzonite;* ***(c)*** *fine to medium-grained biotite hornblende quartz monzonite;* ***(d)*** *fine-grained porphyritic k-feldspar hornblende biotite monzodiorite. Samples (a) DDRCCC-23-041_246.7m, (b) (DDRCCC-23-041_289.2m and (c) DDRCCC-23-041_257.0m are from the Blackjack deposit . Sample (d) DDRCCC-21-009_210.0m is from the Eiger deposit. Inset figures are billet offcuts from corresponding thin sections cut from the sample.*

Fine to medium-grained K-feldspar porphyritic biotite-hornblende quartz-monzonite

A second dike lithology at Blackjack is a light grey, fine to medium-grained K-feldspar porphyritic biotite hornblende quartz-monzonite (Fig. 14c). Phenocrysts are ~0.5 mm across

with 2% of feldspars ranging up to 1 to 3 mm. Modal compositions are approximately K-feldspar (35%), plagioclase (25%), quartz (15%), biotite (10%), hornblende (5%), and disseminated sulphides (up to 5%) consisting of pyrrhotite and pyrite. Contacts are sharp and undulating with no corresponding alteration or chilled margins (Fig. 14c).

Medium-grained equigranular to K-feldspar porphyritic hornblende-biotite monzodiorite to diorite

The main intrusion at Eiger is a dark grey to black, fine to medium-grained, equigranular to K-feldspar porphyritic, hornblende>biotite monzodiorite (Fig. 14d). When porphyritic, phenocrysts of pyroxene, hornblende and plagioclase are euhedral and range from 1 to 2 mm wide. Felsic minerals (~40%) comprise plagioclase (35%), lesser K-feldspar (7%) and quartz (3%). Mafic minerals (55%) consist of hornblende (25%), biotite (20%) and pyroxene (10%). Accessory minerals and sulphides represent 3 to 5%. The groundmass of the finer end member (0.1 to 0.6 mm across) consists of light orange-brown to medium orange-brown subhedral to anhedral biotite (Ti-enriched) intergrown with light to medium green hornblende, plagioclase, lesser K-feldspar and minor quartz (3%; Fig. 15). Polysynthetic twinning and minor zoning are common in plagioclase. Most biotite displays sulphide replacement and dark pleochroic halos from radiation damage by radiogenic minerals such as monazite and zircon. Weak to moderate chlorite after biotite often coincides with rutile needles (Fig. 15). Pyroxene is colourless to pale green, commonly twinned, locally zoned, and forms glomerocrysts (Fig. 15). There are also rare significantly altered mafic xenocrysts (Px + Bt + sulphides) with reaction rims. Sulphides in this sample are predominantly pyrrhotite intergrown with minor pyrite and lesser arsenopyrite.

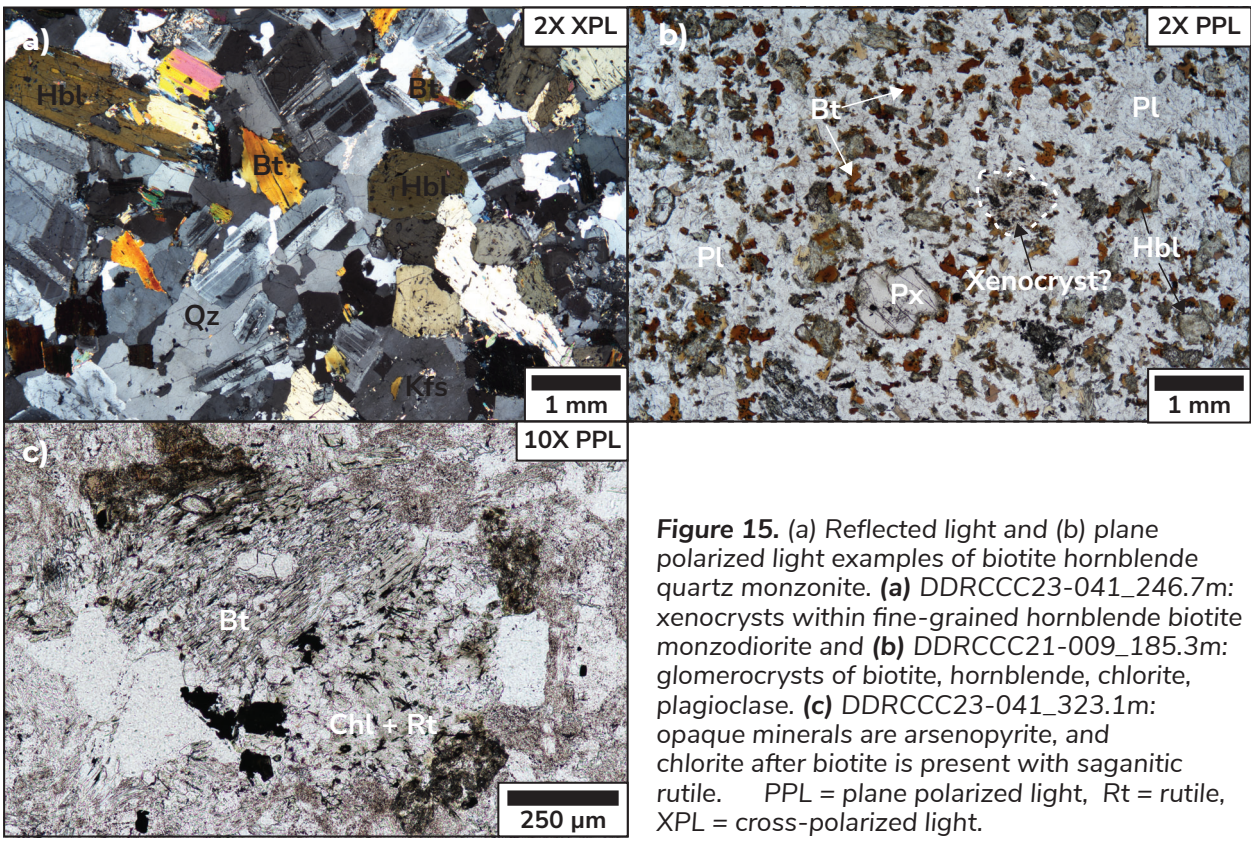

Figure 15. *(a) Reflected light and (b) plane polarized light examples of biotite hornblende quartz monzonite.* ***(a)*** *DDRCCC23-041_246.7m: xenocrysts within fine-grained hornblende biotite monzodiorite and* ***(b)*** *DDRCCC21-009_185.3m: glomerocrysts of biotite, hornblende, chlorite, plagioclase.* ***(c)*** *DDRCCC23-041_323.1m: opaque minerals are arsenopyrite, and chlorite after biotite is present with saganitic rutile. PPL = plane polarized light, Rt = rutile, XPL = cross-polarized light.*

Lamprophyre

Dark grey to black, fine-grained equigranular to biotite-feldspar porphyritic lamprophyric rocks are found at both the Blackjack and Eiger deposits and crosscut all major lithological units. Locally biotite phenocrysts are aligned near dike contacts which are typically sharp and irregular with weakly defined chilled margins on the centimetre-scale. Lamprophyre dikes have abundant secondary carbonate in the groundmass. Intervals observed in drill core lacked significant quartz-veins and have low Au-grades in lamprophyre.

In thin section, all lamprophyres are commonly porphyritic with zoned light honey-brown to brown biotite-phlogopite phenocrysts (Fig. 16b). Pyroxene is typically subhedral to anhedral and commonly forms glomerocrysts, with minor quartz eyes and lesser K-feldspar and hornblende in a fine-grained matrix of predominantly carbonate, K-feldspar and lesser biotite and plagioclase (Fig. 16). The dominant presence of biotite and orthoclase (K-feldspar) suggests they are minette lamprophyres. Lamprophyric whole-rock samples contain 53 to 55% silica.

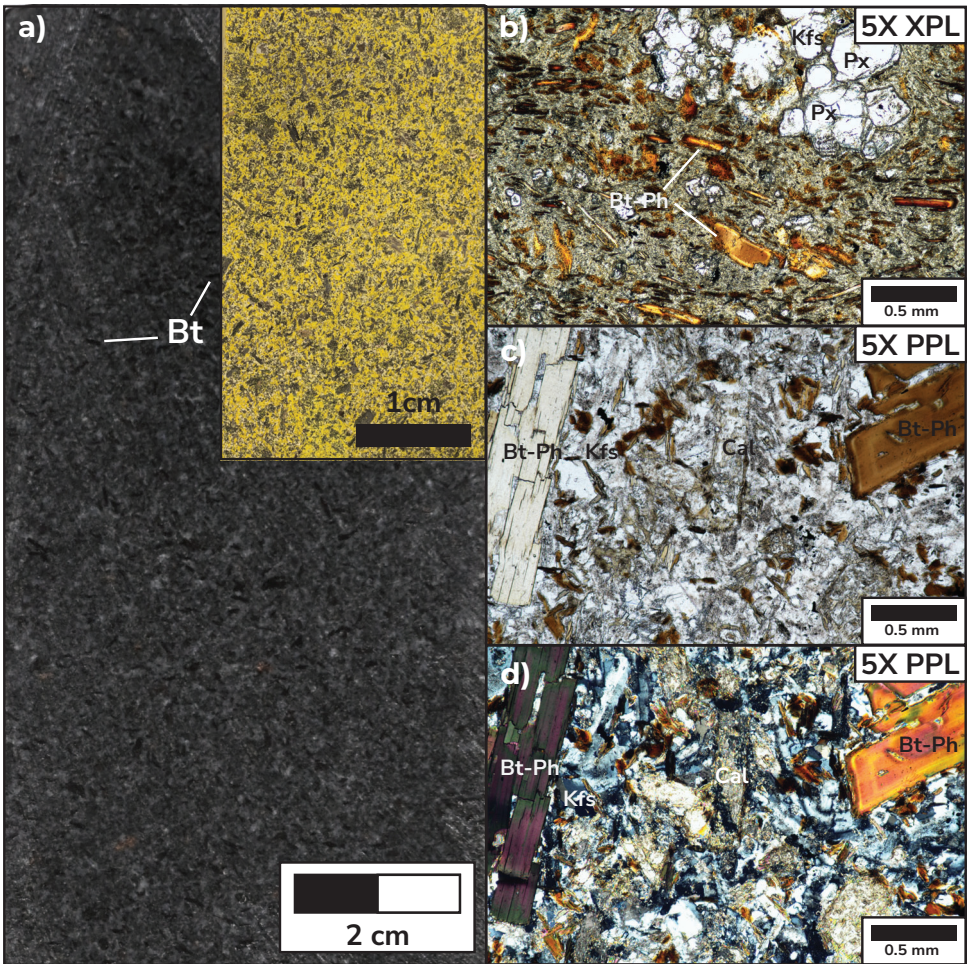

Figure 16. *Lamprophyre examples in drill core (a) and in plane polarized and reflected light (b, c, d). Dark grey to black, fine-grained equigranular to porphyritic biotite feldspar lamprophyres seen at both Blackjack and Eiger and crosscut all major lithological units. Biotite-phlogopite is often honey brown and zoned in thin section, groundmass is predominantly calcite, K-feldspar and lesser biotite and plagioclase. Local alignment of biotite. Clinopyroxene occurs as cumulates with K-feldspar and minor quartz (b). Ph = phlogopite, Kfs = K-feldspar, Cal = calcite.*

Veins, mineralization and alteration

Gold at both Blackjack and Eiger is primarily hosted in sheeted veins 0.5 to 2 cm wide (locally up to 15–20 cm) which crosscut all major lithological units except lamprophyres (Fig. 17). Two dominant orientations of veins are noted at the Blackjack deposit, both vein sets strike between 090° and 110°. The main orientation dips steeply to the south and the second orientation dips moderately to the north. Veins are commonly observed with similar orientations, although crosscutting orientations are present (Fig. 17). Average vein densities range from 3 to 10 veins per metre. At Blackjack, increased Au grades are correlative with increased vein densities, areas with increased textural variability, and areas of subsequent intrusion emplacement within the main K-feldspar biotite-hornblende quartz-monzonite.

Two dominant styles of sheeted veins are observed in both deposits: sulphide-poor (3–5%) quartz veins and sulphide-rich (10–90%) quartz veins. The sulphide assemblage in sulphide-poor quartz veins typically consists of pyrrhotite ± bismuthinite ± arsenopyrite ± pyrite ±

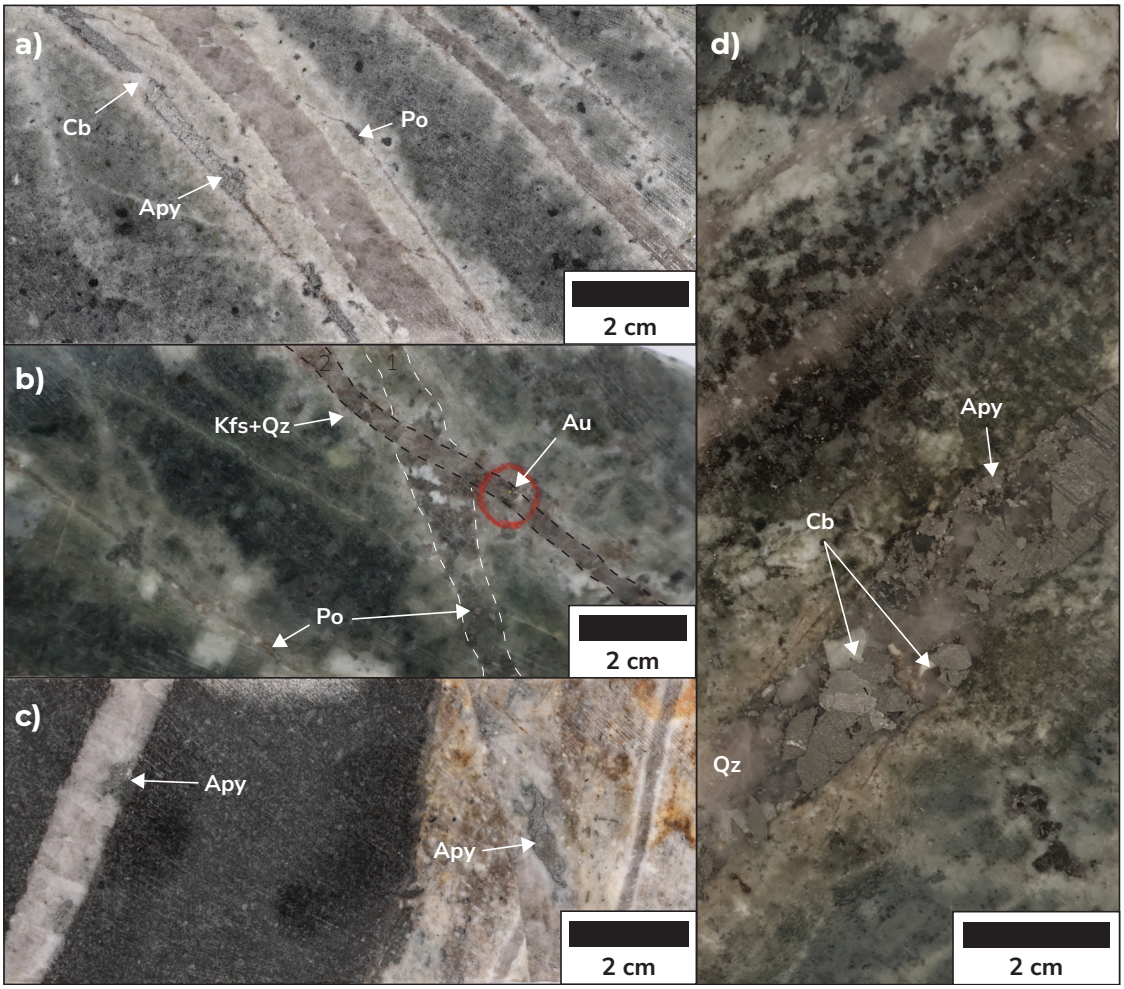

Figure 17. *Examples of mineralized intervals at RC Gold. Samples in (a), (b) and (d) are from Blackjack, sample (c) is from Eiger.* ***(a)*** *Sheeted quartz-arsenopyrite-pyrrhotite-pyrite (<3% sulphide) veins coincident with massive arsenopyrite veins (>80% sulphide).* ***(b)*** *Sheeted quartz-pyrrhotite-arsenopyrite-bismuthinite-Au veins crosscutting quartz-pyrrhotite-arsenopyrite veins in feldspar phyric quartz monzonite. Millimetre-scale feldspar-sericite-quartz in alteration halo. Dark green chlorite-sericite wash across the interval. Visible gold highlighted by red circle.* ***(c)*** *Multiple orientations of quartz-arsenopyrite veins with minor alteration halos. Lithology on the left is hornblende biotite quartz monzodiorite-diorite, right is medium grained aplite dike.* ***(d)*** *Sheeted sulphide-poor quartz veins with similar composition to sample (b) and massive arsenopyrite-quartz-carbonate vein in quartz monzonite.*

scheelite and carbonate (Figs. 16 and 17). Sulphide-rich veins typically comprise 10 to 90% massive arsenopyrite with little to no quartz or carbonate. Both types of veins are similarly oriented, though sulphide-dominant veins often exploit pre-existing sulphide-poor quartz vein structures (Fig. 17). Quartz-pyrite stringers with chlorite-sericite halos, and chlorite-pyrite veins with quartz-feldspar halos, were observed and open space quartz-carbonate veins are rare.

The dominant sulphides and tellurides observed at Blackjack are arsenopyrite, pyrite, pyrrhotite, bismuthinite and bismuth tellurides and minor chalcopyrite. Gold is associated with bismuthinite, native bismuth and bismuth tellurides, typically occurring as free gold adjacent to and within host sulphides (Figs. 17 and 18). In thin section arsenopyrite is commonly observed as pitted grains intergrown with pyrrhotite (Fig. 17).

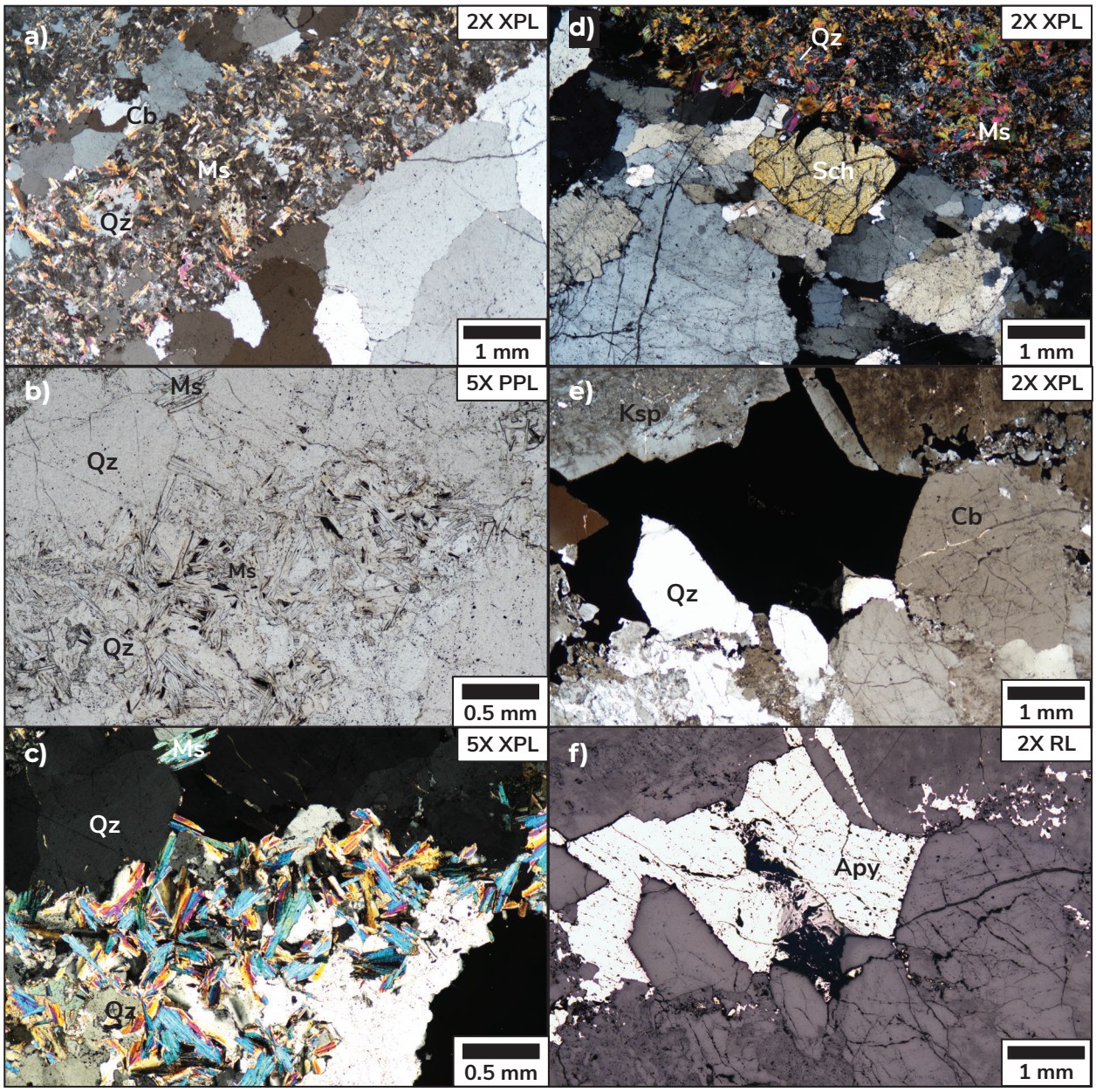

Figure 18. *Plane polarized, cross-polarized and reflected light photomicrographs of mineralized samples at RC Gold. Samples (a) and (b) show quartz-muscovite alteration in vein selvedges. Samples (c) and (e) are coarser grained examples of muscovite and quartz in vein selvedges. Samples (d) and (f) show arsenopyrite within open-space veins. Ms = muscovite.*

Alteration is observed both at a vein-scale, as well as metre to sub-metre scale quartz + sericite alteration fronts associated with faulting and intrusion emplacement. At a vein-scale, alteration halos range from millimetre-scale to several centimetre-scale and typically consist of one or more of albite, quartz, K-feldspar, sericite, chlorite, (±Fe-) carbonate, and lesser disseminated sulphides (arsenopyrite, pyrite and pyrrhotite; Figs. 17 and 18). Where broad alteration halos are present, they are typically characterized by white-green strong, pervasive, quartz and sericite alteration which masks primary textures. Sericite alteration of feldspars and biotite, as well as chlorite alteration of biotite and hornblende is common and often coincident with disseminated pyrrhotite, arsenopyrite and pyrite in vein selvedges and disseminated in surrounding wall rock.

In thin section, alteration associated with sheeted quartz, quartz-sulphide and sulphide-rich veins typically comprises pervasive K-feldspar, muscovite and sericite. Most K-feldspar and plagioclase are completely altered to sericite and secondary K-feldspar and are dirty-brown in plane polarized light. Pale green hydrothermal muscovite is observed flanking most quartz veins locally as euhedral crystals, though also as subhedral to anhedral masses (Fig. 18). Muscovite occurs as larger grains adjacent to the vein boundary and fines outward to sericite into the surrounding wall rock on a centimetre-scale (Fig. 18).

Steiner deposit

Five days were spent logging three holes from 2024 drilling at the Steiner deposit (DG24-1028C, DG24-1029C and DG24-1030C; Fig. 19). Steiner core was logged as a proxy for the Eagle deposit because access to the Eagle deposit core was not possible during the 2024 field season. Steiner is located 700 m northwest of the Eagle pit wall and has similar mineralization to the Eagle deposit, though of a slightly lower grade (Kirk, 2016). Forty-seven representative samples were taken; two were sent for whole-rock analysis, fourteen polished thin sections were made, and five quartered core samples were stained using sodium cobaltinitrate.

Property scale geology

The Steiner deposit is located 85 km NNE of the village of Mayo and 350 km north of Whitehorse (Fig. 1). Yusezyu Formation rocks of the Hyland Group are the country rock to the deposit with the deposit itself related the Dublin Gulch stock (Fig. 3). This stock is a granodiorite intrusion that forms an elongate ridge (6 km × 2 km) along a 070°-trend of the Dublin Gulch antiform (Fig. 19; Kirk, 2016). The global resource at the Eagle Gold Mine is 2.6 Moz Au (Proven and Probable) and 4.4 Moz Au (Measured + Indicated) between their Eagle and Olive deposits (Harvey et al., 2023). At the Olive deposit, 3 km east of Steiner, gold mineralization is dated at 93.2 ± 0.3 Ma (Re/Os molybdenite; Selby et al., 2003).

Intrusive rock descriptions and field relationships

At Steiner, the dominant intrusive host lithology is a green-grey medium-grained equigranular biotite diorite-granodiorite. Volumetrically minor mafic dikes are also present. Intervals of the intrusion in drill core range from 25 to 140 m wide and are often interfingered with surrounding hornfelsed and strongly altered metasediments on a metre to several metre-scale. Lesser 1 to 5 m-wide black-green mafic dikes and fine to medium-grained plagioclase porphyritic dikes, and aplites crosscut the main intrusion. Weak to moderate fracture-controlled and patchy disseminated oxidation was observed in drill core to a depth of 125 m. Metasedimentary rocks are extensive in holes DG24-1028C and DG24-1029C and are only generally described here as they are not the focus of this study. The intrusions at Steiner are metaluminous, magnesian, calc-alkalic and silica-saturated (Fig. 20).

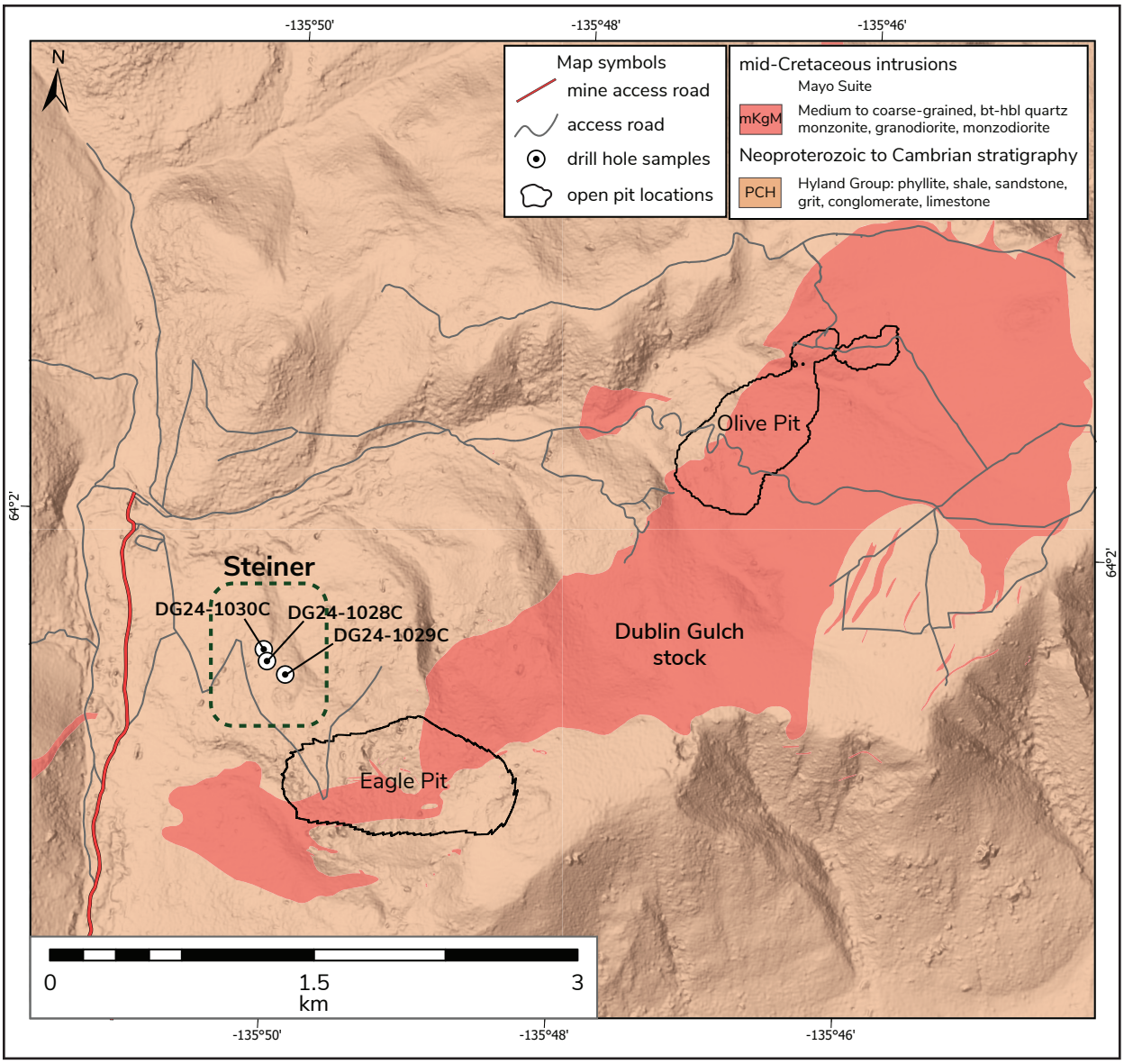

Figure 19. *Simplified Steiner property geology. Property-scale intrusions are from Victoria Gold Corp. (pers. comm, 2020), bedrock geology is otherwise 1:250 000 scale to correlate with Figure 3. Black outlined polygons are open pit locations. White circles represent collars from holes that were logged and selectively sampled.*

Fine to medium-grained, equigranular biotite-hornblende granodiorite

The main host intrusion at Steiner is a green-grey to dark grey, fine to medium-grained equigranular to locally seriate biotite>hornblende granodiorite (Figs. 20 and 21). Phenocrysts of all minerals range from 1 to 5 mm wide and represent 5 to 10% of the rock. Modal compositions are approximately plagioclase (35–40%), quartz (20–25%), K-feldspar (10–15%), biotite (10–20%), hornblende (10–15%), titanite (<1%) and up to 5% but typically <1% disseminated sulphides (pyrite, pyrrhotite) in the groundmass. Where observed, intrusive contacts are faulted and blocky over 1 to 2 m in drill core and locally contain 5 to 25 cm-wide, up to 0.5 m xenoliths of angular biotite hornfels and subrounded, strongly silicified psammitic metasedimentary rocks. Magnetic susceptibility of the intrusion averages 0.317 × 10^{-3} SI units (N=2).

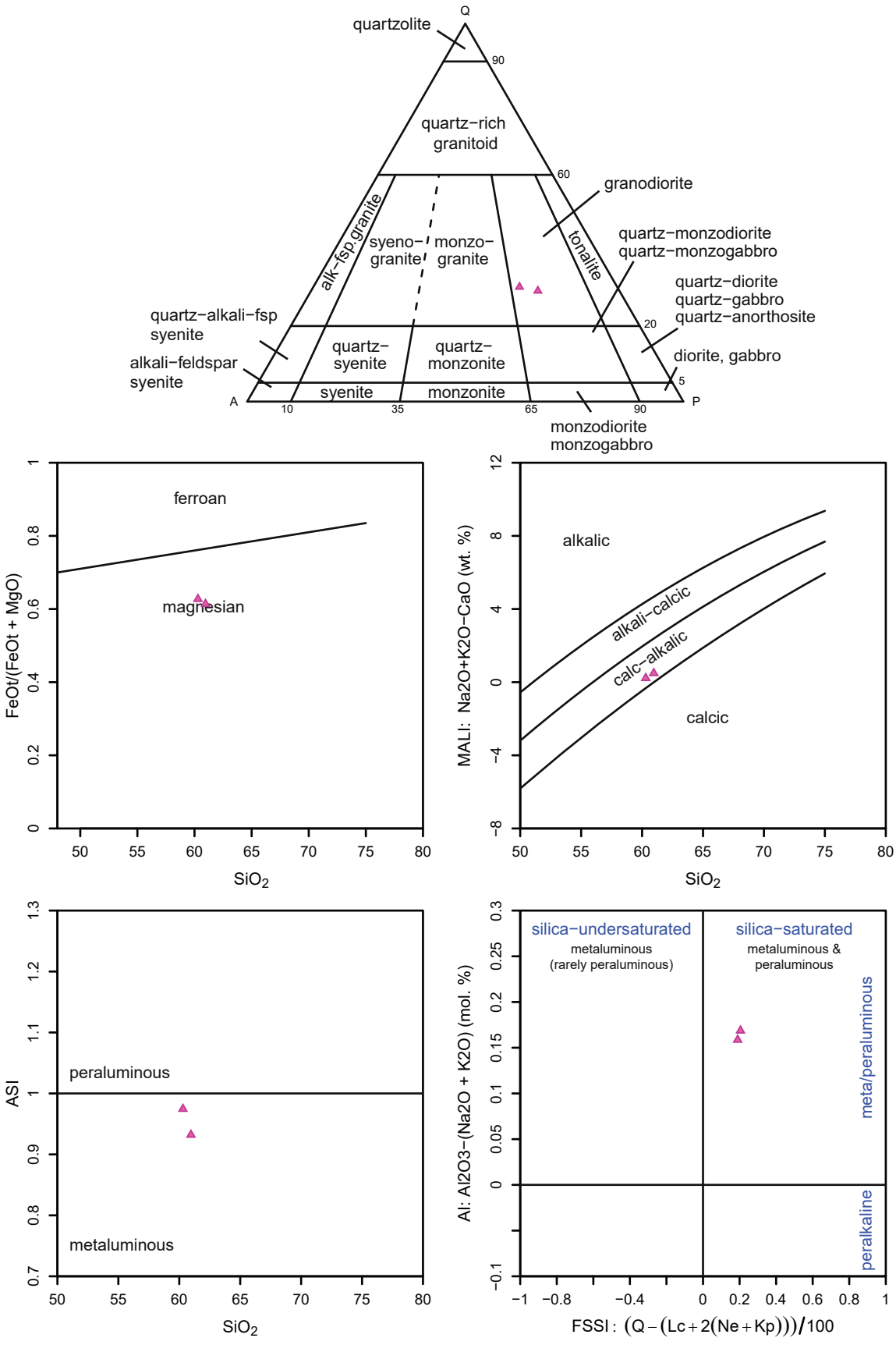

Figure 20. *QAP ternary diagram of Steiner intrusive rocks and Frost and Frost (2008) classification of representative whole rock samples.*

In thin section, plagioclase is subhedral to euhedral, 0.3 to 6 mm across, polysynthetic twinning is common, as is zoning. Mafic minerals are biotite dominant though locally equal amounts of intergrown hornblende and biotite are observed. Hornblende is pale green to light brown, 0.5 to 7 mm across, forms glomerocrysts and is often shredded. Twinning is observed in several hornblende crystals as well as hornblende with rims of biotite. Biotite is light to medium orange-brown, forming sub to euhedral laths, is present in the groundmass (0.4 mm long) and occurs as phenocrysts (~5 mm wide). Sulphides comprise <1% of the rock and consist of pyrrhotite, pyrite and chalcopyrite.

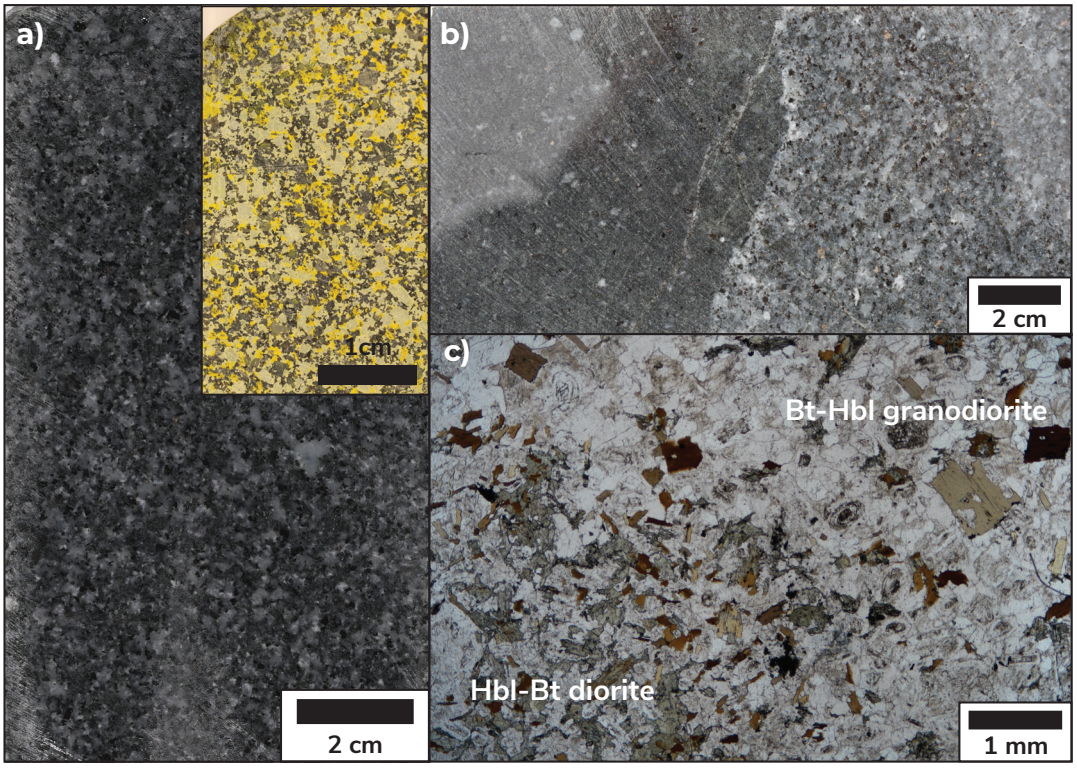

Figure 21. (a) *Medium-grained equigranular biotite hornblende granodiorite (DG241030C_152.8m), and* ***(b)*** *Fine-grained porphyritic hornblende biotite diorite (DG241030C_152.5m) observed crosscutting the main granodiorite intrusion, minor feldspar alteration at the contact. Samples (a) and (b) are from drill core.* ***(c)*** *Plane polarized photomicrograph of the contact between hornblende-biotite diorite (left) and biotite-hornblende granodiorite (right).*

Fine-grained hornblende-biotite porphyritic diorite

A secondary, less volumetrically significant intrusion occurring as dikes is a dark grey, fine-grained plagioclase porphyritic hornblende>biotite diorite (Fig. 21). Groundmass is sub-mm and consists of plagioclase and minor K-feldspar. Approximately 10% of the rock is phenocrysts consisting of 1 to 3 mm wide subrounded to rounded quartz, 1 to 2 mm long euhedral biotite and 1 to 2 mm long subhedral white feldspar. Approximate modal compositions are hornblende (50%), biotite (15–20%), plagioclase (15–20%), K-feldspar (5–10%), quartz (5%), titanite (1–2%) and less than 1% disseminated pyrrhotite. Where observed, contacts with biotite-hornblende medium-grained diorite are sharp with no chilled margins and limited associated alteration (Fig. 21). Mafic enclaves with similar composition were also observed.

Veins, mineralization and alteration

Gold mineralization at Steiner is hosted within sheeted to stockwork veins, which crosscut all intrusive suites and metasedimentary rocks (Fig. 22). Two types of veins are present: sulphide-poor (3–5% sulphides) quartz veins and later sulphide-rich (10 -90% sulphides) ± quartz veins (Fig. 22). The dominant sulphide mineral in veins is arsenopyrite, with lesser pyrite, pyrrhotite and bismuthinite. A late base-metal signature was observed as massive sulphide veins (5–20 cm wide) in drill core consisting primarily of galena, pyrite and sphalerite (Fig. 22).

Sulphide-rich veins consists of massive arsenopyrite with minor intergrown pyrite and blebs of chalcopyrite, titanite and carbonate interspersed within veins. Sulphide-rich veins are typically observed overprinting earlier sulphide-poor veins. Quartz sulphide-poor veins often have intergrown quartz, muscovite, carbonate, sericite and minor titanite. Quartz is dusty due to fluid inclusions and sporadically rutilated.

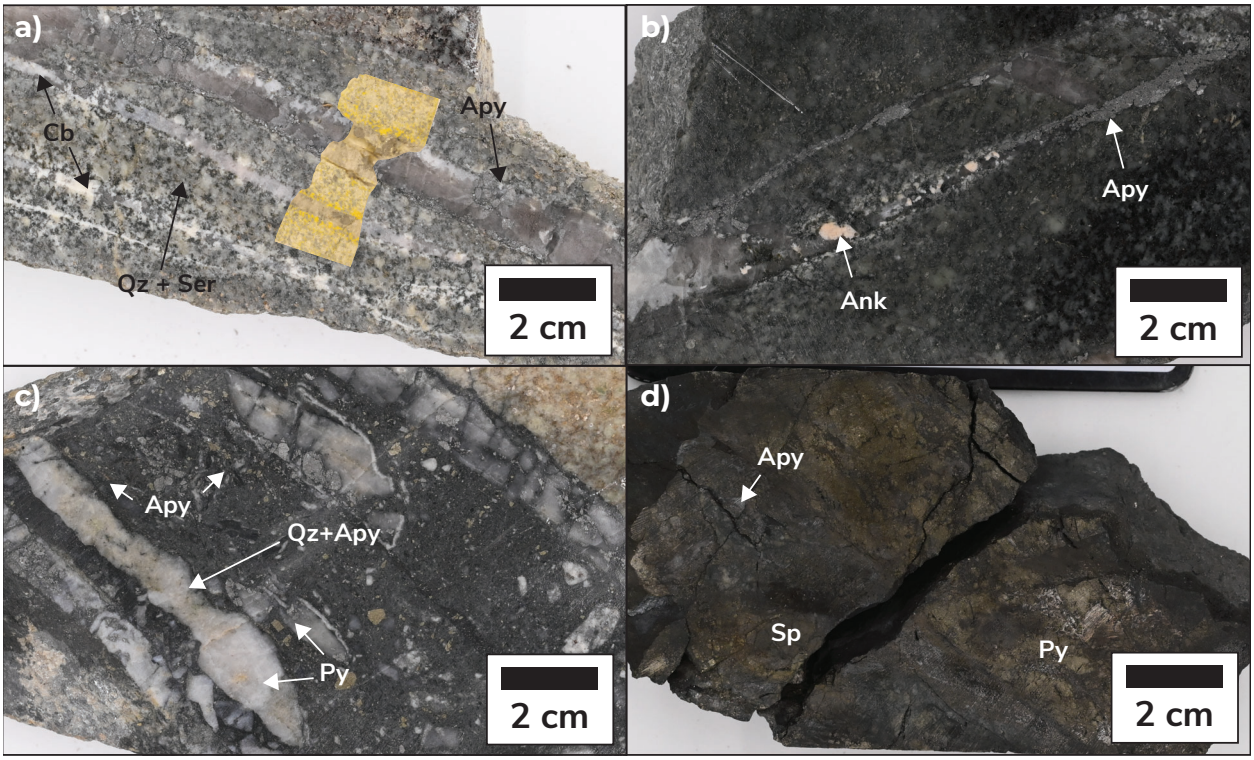

Figure 22. *Examples of mineralized intervals at Steiner. Sheeted quartz-arsenopyrite-carbonate veins in moderately quartz-sericite altered granodiorite.* ***(a)*** *Overlain thin section billet photo highlights potassic alteration (<1 mm) in vein selvedges (DG241030C_204.3m).* ***(b)*** *Arsenopyrite ankerite-quartz veins crosscutting earlier quartz-arsenopyrite-pyrrhotite veins (DG241030C-165.8m).* ***(c)*** *Quartz sulphide cemented breccia with disseminated and euhedral sulphides within the matrix, clasts of quartz-arsenopyrite veins, and quartz-arsenopyrite veins along breccia boundaries (DG241030C_180.5m).* ***(d)*** *A late massive arsenopyrite-pyrite-sphalerite-galena vein (DG241028C_85.3m). Ank = ankerite, Sp = sphalerite.*

Alteration was observed both at a vein-selvedge scale and metre-scale, coincident with increased faulting and where the intrusion is in contact with surrounding metasedimentary rocks. Metasedimentary rocks are commonly intensely silicified and sericitized when psammitic and strongly biotite-hornfelsed when pelitic. Localized pervasive quartz and sericite alteration masks primary textures and bleaches narrow intrusion intervals. Alteration related to faulting and sheeted veins typically extends 0.5 cm to 1.5 m into surrounding wall rock. Zoned alteration halos are common where sheeted sulphide-poor quartz veins and arsenopyrite-dominant veins occupy the same structure (Fig. 23a).

Where multiple vein styles are present, two distinct alteration styles are observed (Fig. 23). Strong K-feldspar + muscovite + quartz and quartz + muscovite ± biotite ± pyrrhotite ± pyrite is often associated with sulphide-poor quartz veins. Strong K-feldspar alteration is brown and alters all felsic and mafic minerals within the alteration selvedge (Fig. 23). The second type of alteration is observed as medium to coarse-grained muscovite intergrown with anhedral quartz (locally microcrystalline) and fine-grained sericite (Fig. 23). This second alteration assemblage contains abundant sericite, minor amounts of interstitial carbonate, is K-feldspar destructive and coincides with sulphide-rich veins (Fig. 23).

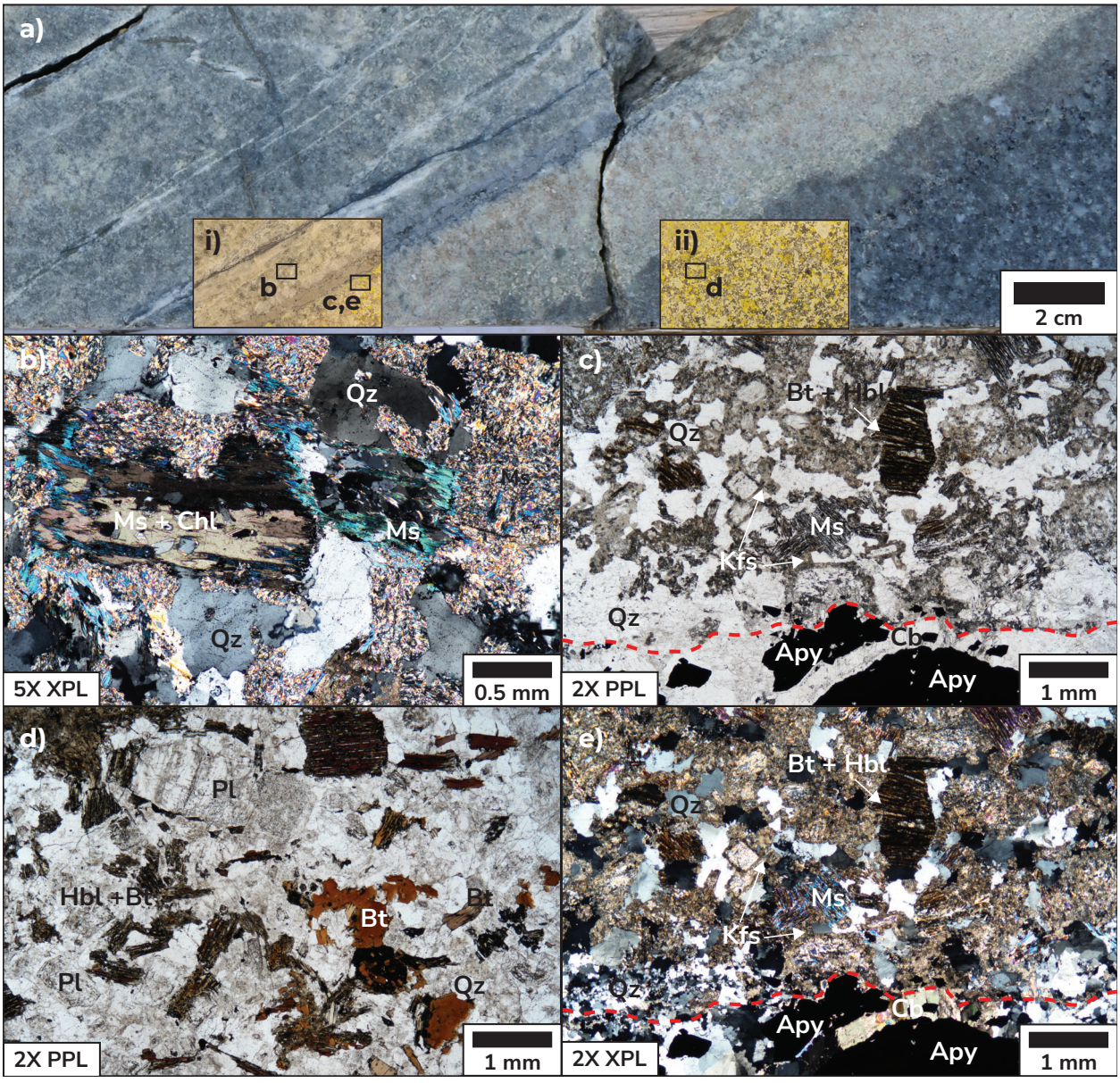

Figure 23. ***(a)*** *Broad alteration halo at Steiner over metre-scale with sheeted quartz-sulphide and sulphide-rich veins in drill core. Inset photos in (a) are sodium cobaltinitrite-stained billet offcuts and contain rectangular outlines of where plane-polarized and cross-polarized photomicrographs (b–e) were taken.* ***(b)*** *Where alteration is K-feldspar destructive, alteration consists of fine to coarse-grained muscovite and anhedral quartz and minor carbonate. Quartz is often recrystallized.* ***(c)*** *plane and* ***(e)*** *cross-polarized photomicrographs of the same location. Red dashed line indicates the boundary of the quartz-carbonate-arsenopyrite vein. Alteration in vein selvedge is predominantly quartz, muscovite, secondary K-feldspar and biotite.* ***(d)*** *Shows weaker biotite-after-hornblende, sericite-after-feldspar, and chlorite-after-biotite alteration ~5–6 cm outside of the vein.*

Valley deposit

Five days were spent on site logging three representative holes of the Valley deposit: one hole from 2023 drilling (V-23-039) and two holes from 2022 drilling (V-22-020 and V-22-010; Fig. 24). The location and orientation of these holes provided an appropriate cross section through the Valley deposit (Fig. 24). Nineteen representative core samples were taken; four were sent to ALS for whole-rock geochemical complete characterization and seventeen polished thin sections were made.

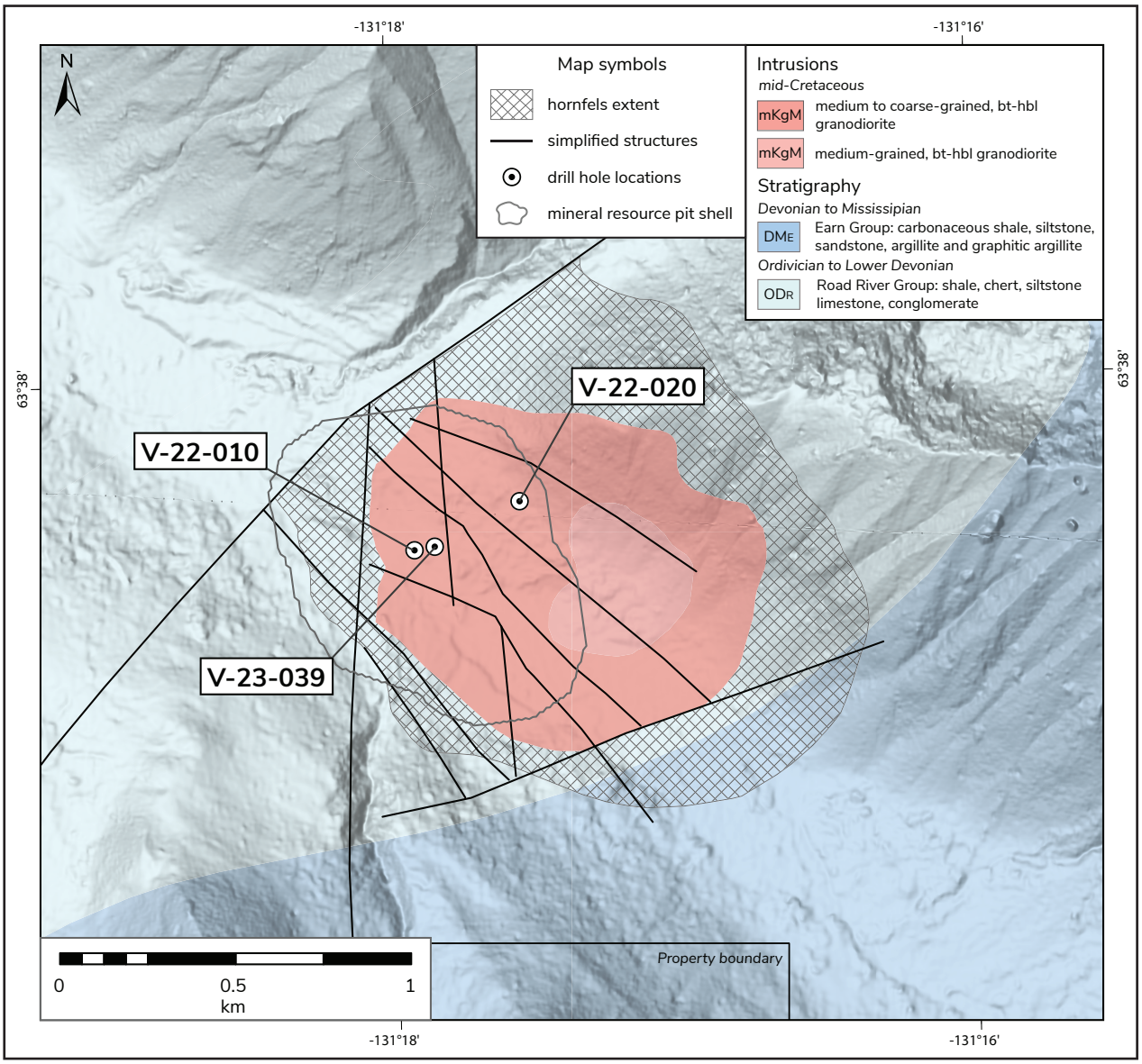

Figure 24. *Simplified Valley property geology. Property-scale intrusions and pit outlines are from Snowline Gold Corp. (pers. comm 2024) ; bedrock geology is otherwise 1:250 000 scale to correlate with Figure 3. White circles represent collars from holes that were logged and selectively sampled.*

Property scale geology

The Valley deposit on the Rogue Project is located in east-central Yukon and is approximately 230 km east of the community of Mayo and 195 km N-NE of the community of Ross River (Fig. 1). The Valley deposit is underlain by Ordovician to Silurian Elmer Creek and Steel

formation and Devonian Portrait Lake Formation of the Earn Group (Fig. 3, Fig. 24; Burrell et al., 2024). All stratigraphy has been tightly folded as part of the Emerald Lake synclinorium and has been subsequently intruded by numerous stocks, plutons and dikes (Burrell et al., 2024). The Valley stock is the focus of this study and is elongated slightly NW and has an 850 by 1100 m footprint at surface (Burrell et al., 2024).

Intrusive rock descriptions and field relationships

At the Valley deposit, there are three main intrusive phases plus volumetrically minor dikes and aplite phases. The Valley deposit is hosted by granodiorite and lesser, later-stage, diorite dikes. All lithological units contain centimetre-scale (2–5 cm, up to 10 cm) dark grey to black fine-grained, locally porphyritic mafic enclaves. Aplites are white-grey, fine-grained feldspar-quartz (± biotite) dikes that are typically 2 to 3 cm wide, but up to 20 to 30 cm wide, and contain 1 to 2% disseminated pyrrhotite and/or pyrite. Aplite dikes crosscut all other lithological units and are often crosscut by mineralized veins. The intrusions are metaluminous to weakly peraluminous, magnesian, and dominantly calcic to calc-alkalic (Fig. 25).

Medium to coarse-grained biotite-hornblende granodiorite

The main host of the Valley deposit is a massive, mesocratic, medium to coarse-grained, equigranular to seriate, biotite>hornblende granodiorite (Fig. 26). Approximate petrographic modal compositions are plagioclase (35%), quartz (25%), K-feldspar (15%), biotite (15–20%) and hornblende (5–10%). Quartz is subhedral to anhedral and commonly has subhedral inclusions of K-feldspar. K-feldspar and plagioclase make up the majority of the groundmass and range from 0.6 to 2.5 mm wide (Fig. 27). Oscillatory zoning is common in plagioclase. K-feldspar shows weak to moderate sericite alteration and plagioclase is weakly to moderately saussuritized. Mafic minerals are primarily biotite and hornblende, and both can have weak to moderate patchy chlorite replacement. Unaltered biotite is pale tan to medium brown, commonly dark brown, whereas hornblende is pale green to medium green, typically subhedral and ragged. Sulphides are observed as intergrowths along grain boundaries or replacing biotite and hornblende. Sulphides are dominantly pyrite with lesser pyrrhotite. Textures of this intrusion locally vary gradationally on a metre-scale, and locally the intrusion contains >50% mafic minerals. Magnetic susceptibility averages 0.493×10^{-3} SI units (N=2).

Fine to medium-grained biotite-hornblende granodiorite

The second most extensive, less mineralized host intrusion is a meso to melanocratic, fine to medium-grained, equigranular to seriate, biotite>hornblende granodiorite (Fig. 26). This intrusion has a similar composition to the main host intrusion but contains less quartz. Approximate petrographic modal compositions are plagioclase (35%), K-feldspar (25%), quartz (15–20%), biotite (15–20%) and hornblende (5%). Phenocrysts vary from sub-mm to 2 mm and represent <5% of the rock. Weak to moderate sericite and chlorite alteration of mafic minerals is common. Carlsbad twinning is observed in most K-feldspars and polysynthetic twinning is common in plagioclase. Minor disseminated sulphides (3–5%) comprising pyrrhotite, pyrite and lesser arsenopyrite are found in the groundmass. Pyrite is commonly observed intergrown with both pyrrhotite and arsenopyrite. Increased quartz-sericite alteration and faulting are observed near contacts with this intrusion and the main granodiorite host, veins crosscuts both intrusions. Magnetic susceptibility averages 0.417×10^{-3} SI units (N=2).

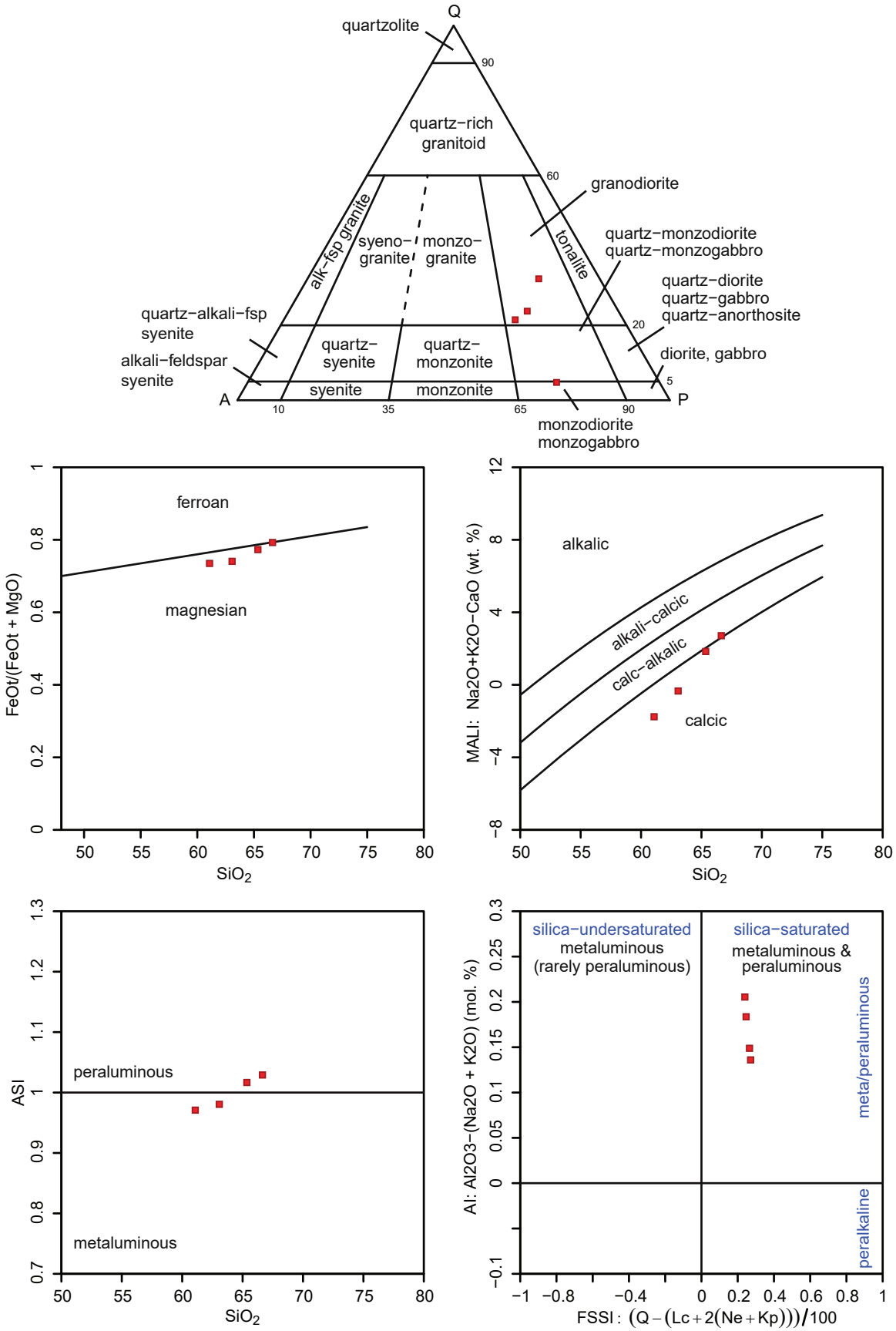

Figure 25. *QAP ternary diagram of Valley intrusive rocks and Frost and Frost (2008) classification of representative whole rock samples.*

Fine-grained porphyritic feldspar-quartz monzodiorite

Both granodiorite phases are cut by a NW-trending dark grey-black, melanocratic fine-grained biotite-hornblende porphyritic monzodiorite (Fig. 26). Fine-grained porphyry intervals are observed as dikes, <50 cm up to 3 m wide and intrude both granodiorite intrusions mentioned above. No significant alteration or chilled margins are observed near contacts.

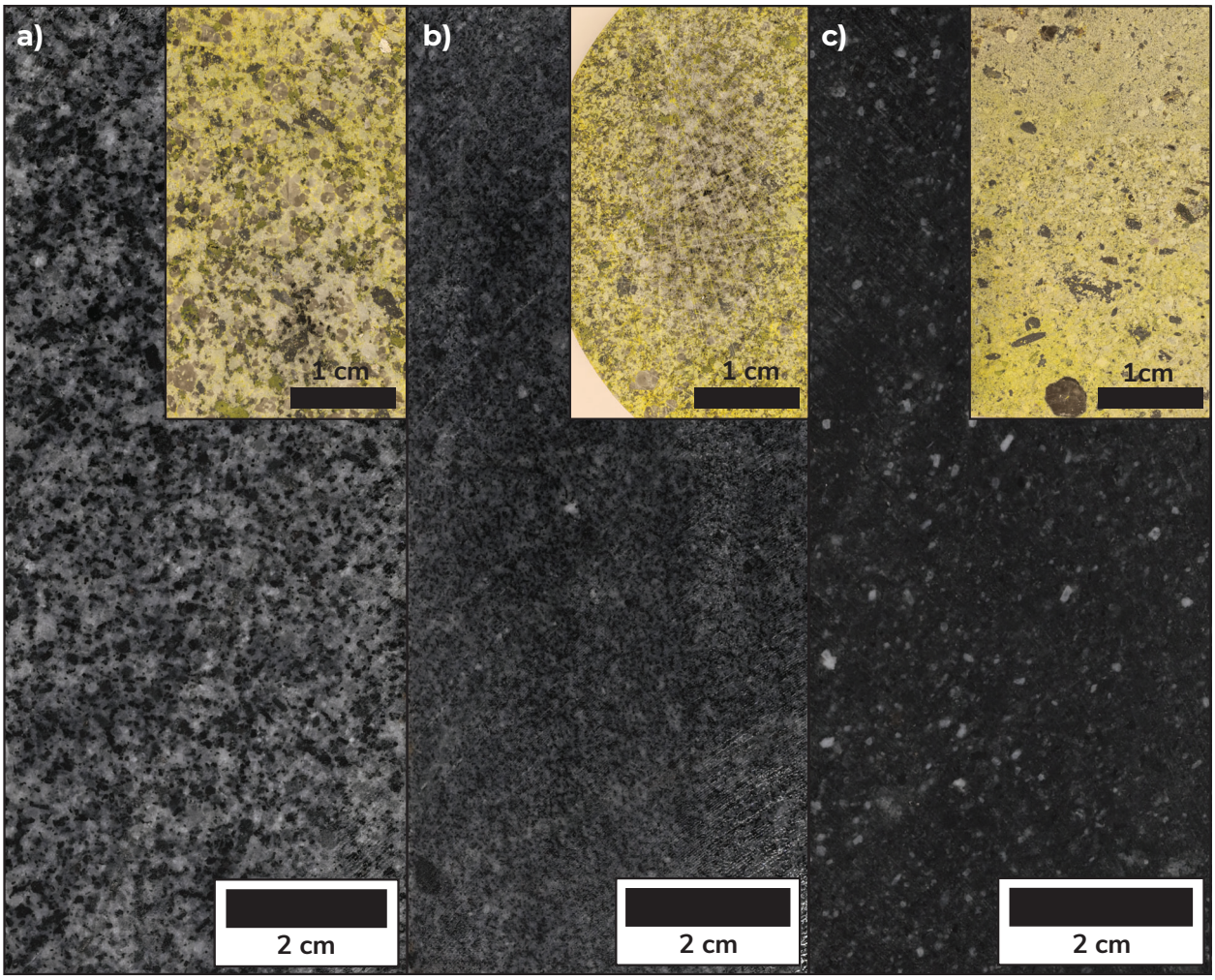

Figure 26. ***(a)*** *Medium-grained biotite-hornblende granodiorite, V-22-020_12.6m,* ***(b)*** *fine to medium-grained biotite-hornblende granodiorite, V-22-020_323.4m, and* ***(c)*** *fine-grained porphyritic feldspar quartz monzodiorite, V-22-020 330.0m. Inset figures are sodium cobaltinitrite-stained billet offcuts from corresponding thin sections cut from the sample.*

Approximate petrographic modal compositions are plagioclase (45%), hornblende (22%), biotite (15%), K-feldspar (15%) and quartz (3%). Quartz is anhedral and commonly embayed. The groundmass consists of 0.05 to 0.1 mm grains of medium brown hydrothermal biotite intergrown with subhedral to euhedral plagioclase. Hornblende is light-medium green, anhedral, and commonly partially or completely replaced by biotite. Weak patchy chlorite replaces biotite and hornblende. Disseminated sulphides (3–4%), locally up to 5%, consist of pyrrhotite, chalcopyrite and pyrite (Fig. 27). Magnetic susceptibility averages 0.971×10^{-3} SI units (N=1).

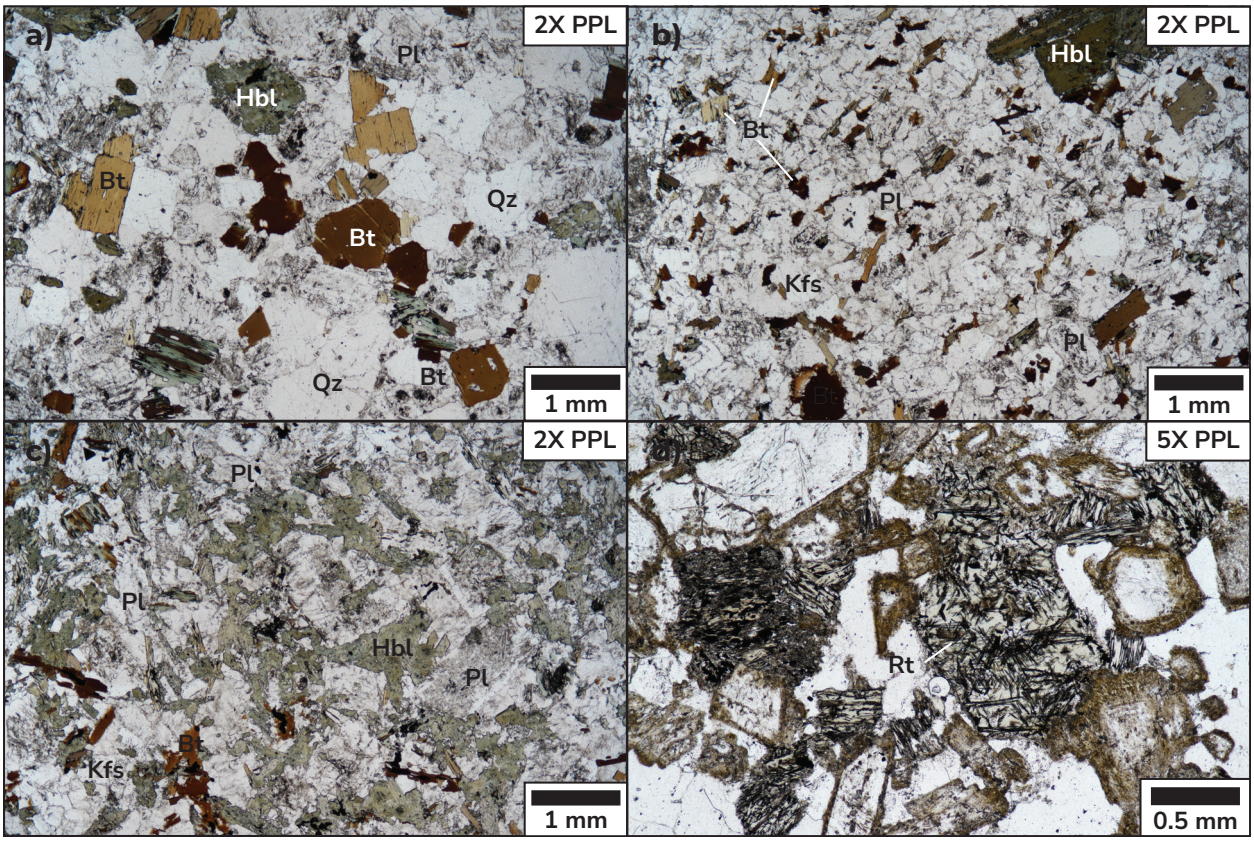

Figure 27. *Photomicrographs of Valley deposit intrusive host rocks.* ***(a)*** *Equigranular biotite hornblende granodiorite, V-22-020_12.6m. Minor chloritization of mafics, feldspars are browner in plane polarized light than quartz. The opaque mineral inclusions in biotite and hornblende are predominantly Po and Py.* ***(b)*** *Fine to medium-grained biotite-hornblende granodiorite, V-22-020_330.3m.* ***(c)*** *Fine-grained hornblende-biotite quartz monzodiorite, V-22-020_139m.* ***(d)*** *Potassic and sericite alteration around rims of feldspars, chlorite after hornblende and biotite, saganitic rutile in altered mafics, V-22-020_183.3m.*

Veins, mineralization and alteration

Gold at the Valley deposit is predominantly hosted within sheeted to stockwork veins that crosscut all major lithological units observed at the deposit. Gold is less commonly disseminated in the surrounding wall rock adjacent to veins (Figs. 28 and 29). Most mineralized veins trend between 280 and 300° and dip steeply 75–80° NE, and locally trend 345° near the intrusive-hornfels contact (Burrell et al., 2024), although at least four orientations of mineralized veins are documented at the deposit. Increased grades are correlative with increased vein densities, intersections of multiple orientations, and locally near faulted intervals.

The dominant sulphides observed at the Valley deposit are pyrrhotite, pyrite, bismuthinite, bismuth and bismuth alloys, and lesser amounts of molybdenite, arsenopyrite and chalcopyrite (Fig. 29). Gold is most commonly observed with bismuthinite, native bismuth and bismuth tellurides, typically occurring as free gold adjacent to and within host sulphides (Figs. 28 and 29). Veins are typically 0.5–1.5 cm wide (up to 20 cm wide) and commonly have sharp margins, are straight-sided and contain <3 to 5% disseminated sulphides. Sinuous, banded or composite and sulphide-rich veins are also observed in drill core (Fig. 28). Where crosscutting relationships are noted, sinuous and discontinuous veins are crosscut by straight, sharp-sided veins, which are later crosscut by sulphide-rich veins.

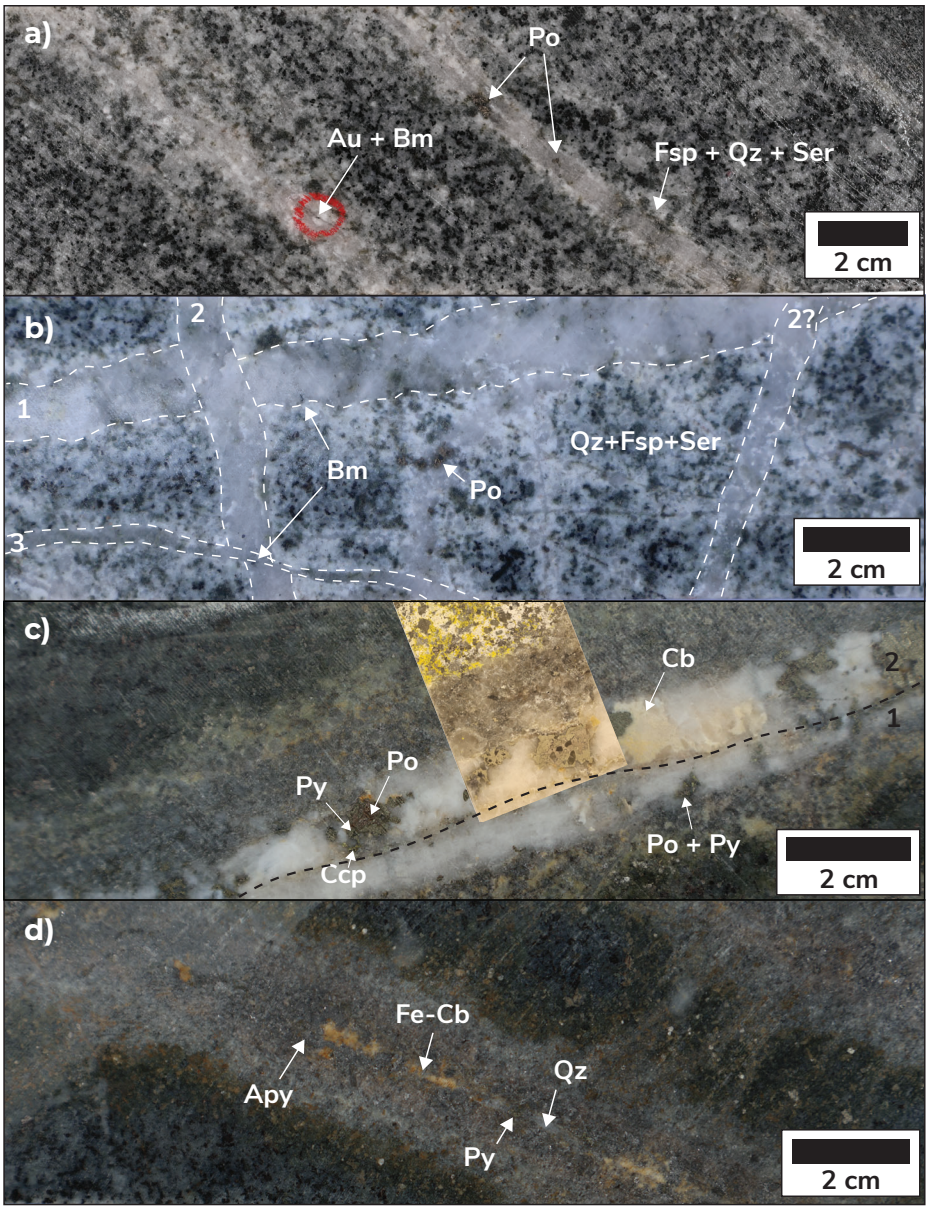

Figure 28. *Examples of mineralized intervals from the Valley deposit.* ***(a)*** *Sheeted quartz-pyrrhotite-bismuthinite-gold veins with minor feldspar-quartz-sericite in vein selvedge characteristic of the deposit (V-23-039_111m).* ***(b)*** *Crosscutting relationships (stockwork) of quartz-pyrrhotite-bismuthinite-gold veins highlighting different vein morphologies and textures, V-23-039_311m. Labels indicate timing. Vein 1 is sinuous, with diffuse boundaries, crosscut by later, straight sided veins (2), which are later offset by millimetre-scale quartz-sulphide veins (3). Feldspar + quartz + sericite alteration in vein selvedges.* ***(c)*** *Quartz-pyrrhotite-pyrite vein structure (1) exploited by secondary quartz-carbonate-pyrrhotite-pyrite vein (2), V-22-020_183.4m. Overlain sodium cobaltinitrite-stained thin section billet highlights the K-feldspar destructive alteration halo crosscutting K-feldspar-quartz-muscovite-biotite alteration halo.* ***(d)*** *Clotted arsenopyrite-pyrite-pyrrhotite-iron-carbonate-quartz vein with zoned alteration halo in distal part of system, V-22-020_450m. Bm = bismuthinite.*

Alteration is typically restricted to vein selvedges (<0.5-5 cm wide outboard of the vein boundary, locally up to 10 cm, Fig. 28) though increased alteration adjacent to fault zones is commonly observed. Alteration minerals in vein selvedges are variable, typically consisting of a combination of K-feldspar and/or albite, quartz, muscovite, sericite, biotite and chlorite (Figs. 28 and 30). K-feldspar (potassic) and in some cases albitic-dominant vein alteration halos appear to be more restricted spatially though are more commonly associated with increased vein

densities and higher gold grades. Alteration assemblages consisting of quartz ± muscovite/sericite ± chlorite ± pyrrhotite ± pyrite as well as chlorite + sericite extend more broadly into surrounding wall rock and are more common in vein selvedges of sulphide-rich veins (Fig. 30). Zoned alteration halos are outboard of the core of the deposit and typically coincide with quartz-sulphide veins that contains more than 3 to 5% sulphides (Figs. 28 and 30).

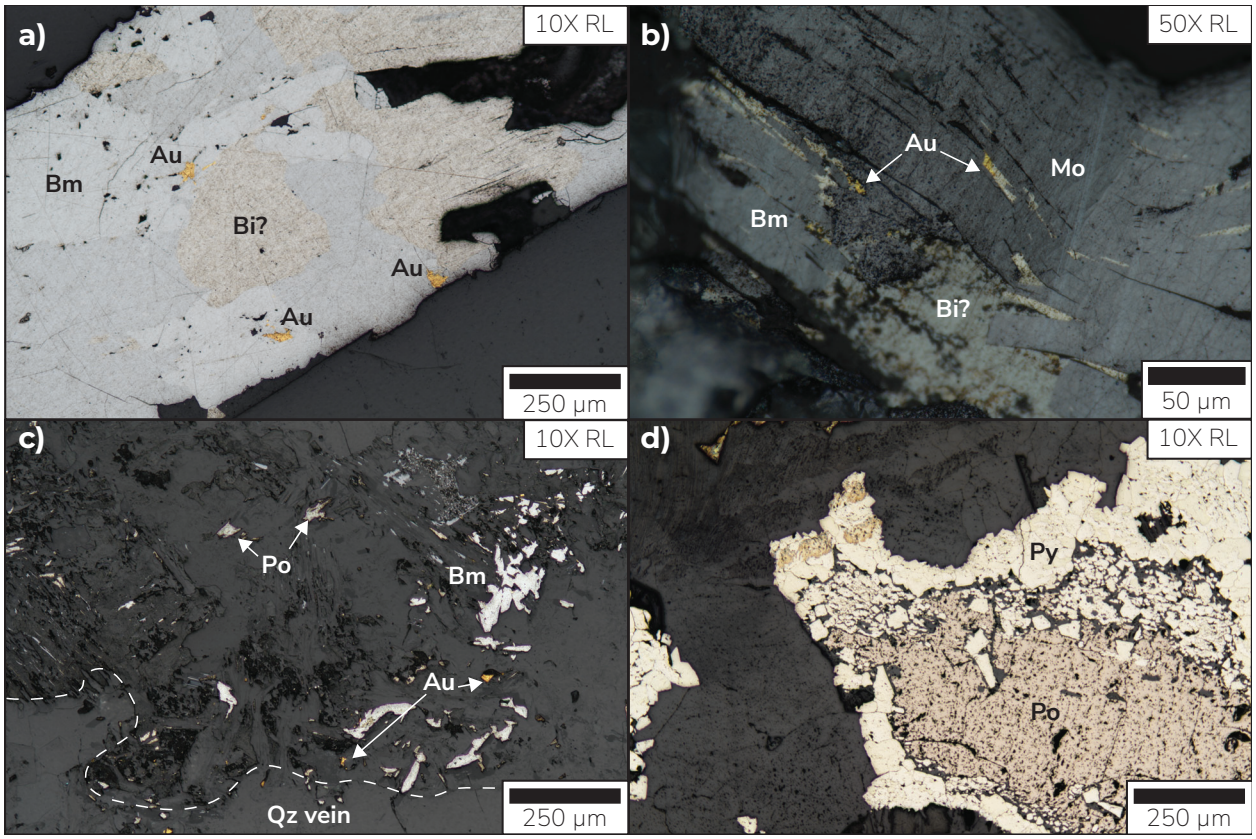

Figure 29. *Reflected light photomicrographs of gold and sulphides in mineralized intervals.* ***(a)*** *Gold in bismuthinite and bismuth sulphides, V-23-039_431m.* ***(b)*** *Gold in molybdenite, bismuth, bismuthinite sulphides, V-23-039_129.4m.* ***(c)*** *Gold, bismuthinite, pyrrhotite disseminated in altered vein selvedge of a quartz-pyrrhotite-bismuthinite-gold bearing vein, V-23-039_431m. White dashed line highlights the vein boundary.* ***(d)*** *Intergrown pyrite replacing pyrrhotite in later sulphide 'rich' quartz vein, V-22-020_183.3m. Bm = bismuthinite.*

Where paragenetic relationships are noted, later sulphide-rich quartz veins exploit and crosscut early sulphide-poor veins. This relationship is also observed in the vein selvedges where later alteration overprints that from early sulphide-poor veins. In thin section, late vein selvedge alteration is characterized by coarse muscovite, quartz, ± carbonate, pyrrhotite and pyrite, and is K-feldspar destructive (Fig. 30). Muscovite is subhedral to euhedral, bladed, and when interstitial it often displays radial textures (Fig. 30). Outer parts of the halo are characterized by brown, moderate to strong K-feldspar alteration, marked by an increase in coarse muscovite and K-feldspar-altered feldspars and hydrothermal biotite (Fig. 30). Hydrothermal biotite is commonly dark brown and often contains rutile. Rutile is present in many strongly altered remnants of mafic minerals. Sulphides are preferentially disseminated and/or replace strongly altered mafic minerals (Fig. 30).

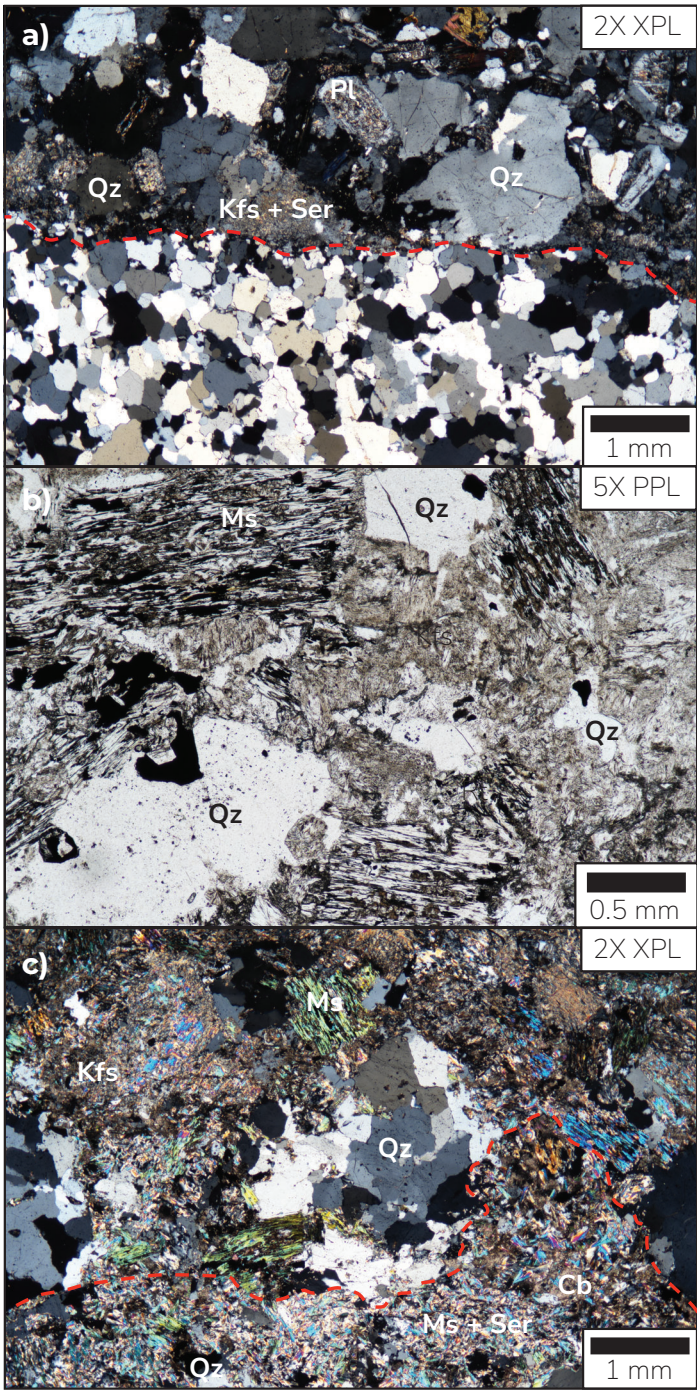

Figure 30. *Photomicrograph examples in plane and cross-polarized light.* ***(a)*** *Finely crystalline quartz-sulphide vein with K-feldspar-sericite-quartz alteration selvedge within granodiorite, V-22-010_254.3m. Preferential alteration in cores of plagioclase is observed in most grains.* ***(b)*** *Highlights coarse muscovite-K-feldspar-quartz±biotite (potassic) alteration in vein selvedge associated with gold-bearing quartz sulphide veins, V-22-020_183.3m. Opaque minerals are predominantly pyrrhotite intergrown with pyrite, minor chalcopyrite.* ***(c)*** *Highlights the transition observed in Figure 28c with inner quartz-muscovite-carbonate-pyrrhotite-pyrite alteration (K-feldspar destructive) overprinting K-feldspar-muscovite-quartz-biotite (potassic) alteration, V-22-020_183.3m. Red dashed line marks the change in alteration assemblages.*

Discussion

Across the four deposits in this study, the sampled intrusions are all silica-saturated containing between 53 and 65% silica (Figs. 7, 13, 20, 25). Intrusions are metaluminous to weakly peraluminous and dominantly magnesian (calc-alkaline; Figs. 7, 13, 20, 25 and Appendix B). The intrusions span the modified alkali lime index (MALI) from alkalic through to calcic and broadly decrease in alkalinity from the west (Brewery Creek's Reserve trend and Classic zone) to the east (Valley), with a similar west-east trend observed in the alumina saturation index (ASI) from metaluminous to peraluminous (Figs. 7, 13, 20, 25 and Appendix B). The Classic zone at Brewery Creek is commonly up to 90% alkali (K) feldspar and plots significantly more alkaline than the biotite-hornblende quartz-monzonite at the Reserve trend.

Major element plots versus SiO_2 highlight broad similarities and differences across the TGB (Fig. 31). Intrusions consistently display a correlation between SiO_2 and CaO, Na_2O, MgO and P_2O_5, and conversely display little correlation between SiO_2 and Al_2O_3, K_2O, FeOt and TiO_2 (Fig. 31). Primitive mantle-normalized rare earth element plots of all deposits are strongly enriched in large ion lithophile elements and light rare earth elements (Fig. 31). All intrusions have distinct negative Nb and Ti anomalies and minor negative Sm anomalies. Classic zone K-feldspar syenite samples (Brewery Creek) show positive anomalies in Zr and Hf (Fig. 31).

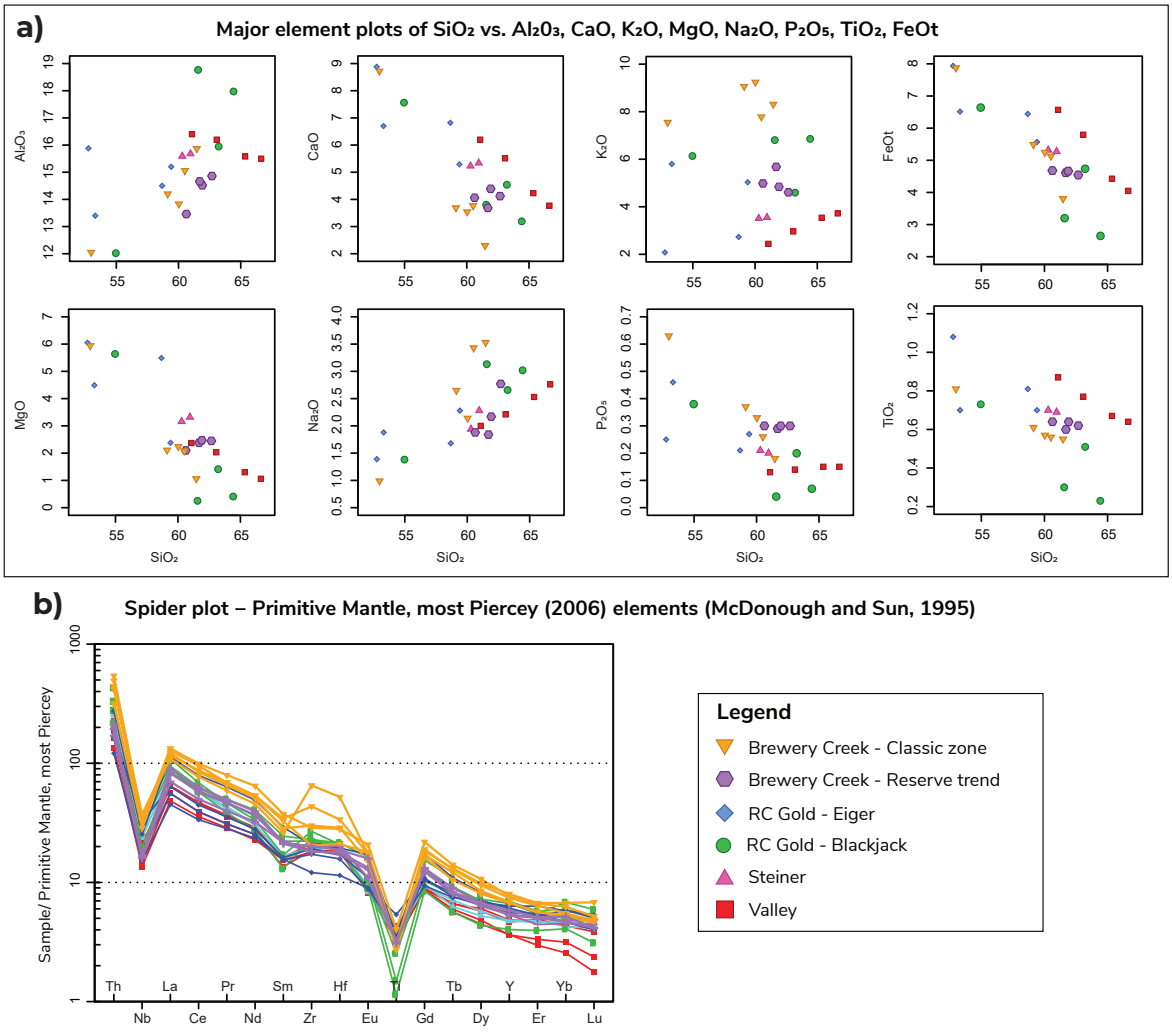

Figure 31. *Whole rock geochemistry results from all deposits.* **(a)** *Harker diagrams (major element plots) of SiO_2 vs major elements.* **(b)** *Rare earth element spider plot (McDonough and Sun, 1996) using most Piercey (2006) elements normalized to primitive mantle.*

The compositions of the intrusions hosting the deposits on the four properties in this study range from granodiorite to diorite, and from quartz-monzonite to quartz-syenite. The Mayo suite intrusions across the TGB typically have modal minerals biotite>hornblende although more mafic phases have greater hornblende ± pyroxene abundance than biotite. Plutons at each deposit are all composite granitoids and thus broadly similar, but in detail each pluton displays evidence for dynamic magmatism as observed by multiple intrusive phases or the presence of microgranular enclaves or autoliths. Autoliths are typically fine grained, rounded to subrounded and locally porphyritic mafic enclaves with diffuse boundaries. This suggests both the enclave and surrounding intrusion were near solidus temperatures, possibly due to entrainment at depth or from magma mingling and injection of mafic magmas (Barbarin and Didier, 1992; Vernon, 1984). Lamprophyres in the reduced intrusion-related model provide evidence of mantle-derived magmas in the system and are typically late to post-mineralization (Rock et al, 1989, Fig. 5). The only lamprophyres that were identified as part of this study were at the RC Gold project (Fig. 16); these were observed crosscutting all host rocks, often contained mafic xenocrysts, and were notably unmineralized.

In the more typical intrusion-hosted deposits (RC Gold [Blackjack, Eiger], Steiner, Valley), the majority of the gold is hosted within extensional, sheeted to stockwork, straight, sharp-sided quartz-sulphide veins with 3–5% sulphide minerals. Sulphide minerals typically comprise pyrrhotite, pyrite, bismuthinite and bismuth alloys, molybdenite, chalcopyrite and arsenopyrite. There is more arsenopyrite observed at the deposits in the west (Steiner, RC Gold, Brewery Creek) than Valley which has more pyrrhotite. Crosscutting relationships between veins and alteration were best documented at the Valley deposit. However, sulphide-rich veins crosscut sulphide-poor veins consistently across all deposits.

Textural variability of quartz-sulphide veins, sulphide-dominant veins, and vein-associated alteration appear to display some consistency across each of the deposits. Preliminary field and petrographic observations suggest that the alteration zonation in RIRG vein selvedges display similar alteration patterns as observed in a porphyry system. Where earlier higher temperature veins typically have associated sodic to potassic alteration in vein selvedges more proximal to the core of porphyry system, later, typically more distal and lower temperature veins are commonly associated with sericitic or phyllic alteration assemblages (Seedorff et al., 2005). Some generations of quartz-sulphide veins observed in this study are sinuous with sugary textures and commonly have diffuse vein boundaries. At the Valley deposit, sinuous veins are observed crosscut by typical sheeted (extensional) veins (Fig. 28c). These sinuous veins resemble A-type veins in a porphyry system which are typically indicative of early, higher temperature and deeper parts of the system associated with initial depressurization of the fluid (Seedorff et al., 2005; Rusk et al., 2008). Sinuous veins are typically spatially related to and commonly crosscut by extensional veins with similar vein selvedge alteration (Fig. 32a). Sheeted to stockwork extensional veins in reduced intrusion-related gold deposits occur as 0.5 to 2 cm wide veins with 3 to 5% sulphides and sometimes display banded and weak centerline sulphide development (Fig. 32b). These textures are notably similar to B-type veins in a porphyry system (Seedorff et al., 2005), however; they do not strictly fit the classification as the sulphide centreline observed in the RIRG extensional veins are typically underdeveloped relative to those in porphyry deposits. Sulphides in quartz veins are instead often observed along vein boundaries and throughout the vein as subhedral to euhedral crystals. Pyrite, pyrrhotite and arsenopyrite stringer veins are commonly found associated with sericite + chlorite alteration halos which are similar to D-type veins in a porphyry system that form as the system cools and becomes progressively more acidic (Seedorff et al., 2005; Fig. 32d).

Pervasive alteration footprints are uncommon in RIRG deposits; however, preliminary field

and petrographic observations show a correlation between vein textures and associated alteration halos, and proximity to the centre of the defined deposits. Alteration associated with proximal sulphide-poor quartz veins is variable and sometimes absent, though typically comprises potassic alteration (K-feldspar ± albite ± muscovite ± quartz ± biotite). Alteration in vein selvedges associated with later, lower temperature sulphide-rich quartz veins overprints K-silicate alteration, is K-feldspar destructive, and typically consists of muscovite/sericite, quartz, chlorite and pyrrhotite/pyrite (Figs. 23, 28, 32). This latter assemblage is characteristic of later acidic phyllic alteration observed in porphyry deposits (Seedorff et al., 2005).

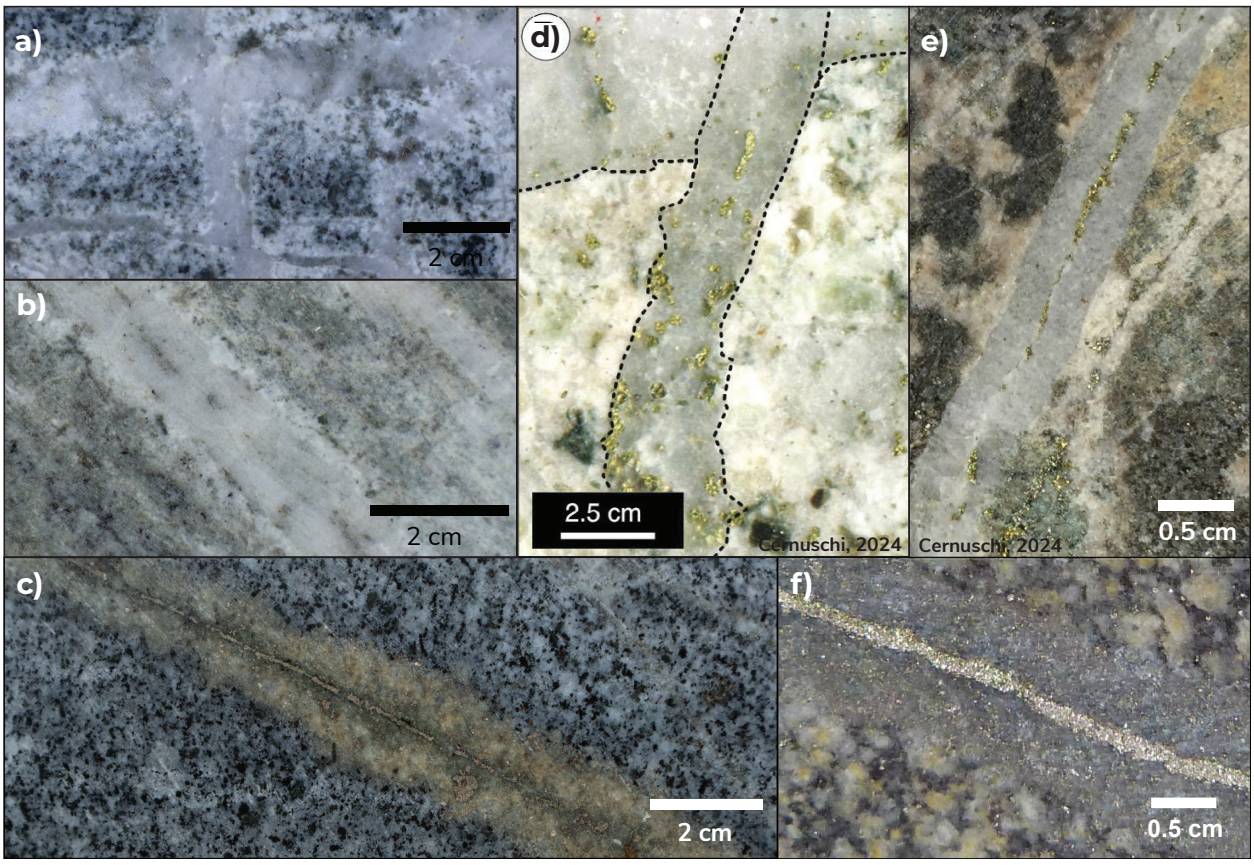

Figure 32. *Examples of reduced intrusion related veins (a, b, c) and Cu-Mo porphyry veins (d, e, f; from Cernuschi et al., 2024), highlighting similarities of vein textures. Quartz-sulphide veins with sinuous morphology, locally diffuse boundaries (a, d) show similarities to A-type veins in a porphyry system. Sharp sided, straight sulphide veins (b, e) are best representative of reduced intrusion-related gold mineralization, weak development of sulphides along centerline (b) are similar to B-type veins in porphyry systems (e). Late and distal pyrrhotite-pyrite veins with chlorite-sericite alteration halos (c) resemble D-type veins in a porphyry system (f).*

RIRG deposits are formed under different structural controls than a typical Cu-Mo-Au porphyry system, i.e., a regional extensional stress regime with generally more lithostatic pressure and with no meteoric fluid interaction (Hart et al., 2004). RIRG deposits appear to share some similarities to porphyry deposits including alteration in vein selvedges, vein textures and spatial distribution of vein types (Fig. 33). In typical Cu-Mo-Au porphyry systems, A-type and B-type veins are associated with potassic alteration domains in the centralized, hotter part of the hydrothermal system which coincides with most of the metal endowment in the system (Seedorff et al., 2005, Rusk et al., 2008). Later sulphide-rich veins (both quartz-sulphide and pyrite-pyrrhotite sulphide stringers) typically have phyllic alteration associated within their

vein selvedges, which are present both distal to the central hydrothermal system as well as crosscutting earlier veins, indicative of the system cooling (Seedorff et al., 2005, Rusk et al., 2008). Each of the RIRGS in this study display dynamic magmatic influx with overprinting intrusive phases which could influence subsequent fluid emplacement and focus or enhance the endowment in specific domains of a mineralizing system. The similarities in vein textures, vein selvedge alteration, and their distribution relative to the core of the system in the deposits in this study could have significant implications for exploration strategies. Identifying textural changes in veins, together with mineralogical composition of veins, vein densities and alteration in vein selvedges may provide another method to determine proximity to an economic mineralizing system.

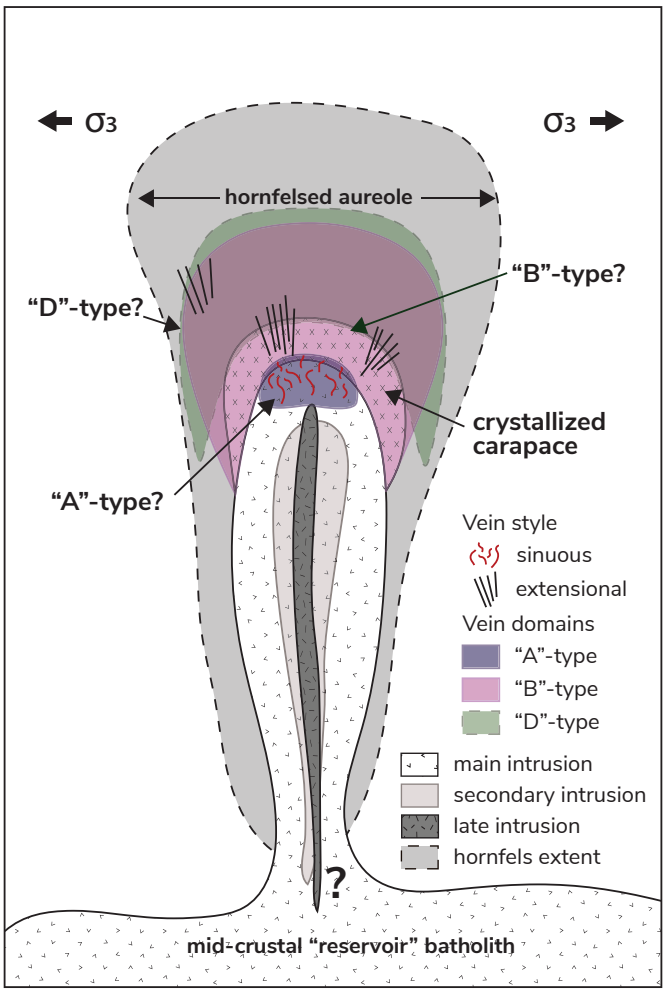

Figure 33. *Hypothetical cross section of a reduced intrusion related gold system with subsequent magmatic phases modified from Hart (2007). Asymmetrical hornfels aureoles are common, and preferred locations of sheeted to stockwork veins are within the carapace of the intrusion. Overlain are preliminary interpretive domains of the distribution of A-type (sulphide-poor quartz vein, sinuous with diffuse vein boundaries), B-type (sulphide-poor quartz vein, straight sided sheeted to stock work veins) and D-type (sulphide dominant veinlets/stringers) vein domains. Sulphide-rich quartz veins (e.g., arsenopyrite dominant) are later and appear to overlap "A" and "B"-type vein domains.*

Future work

Reduced intrusion-related gold systems are underrepresented in scientific literature and therefore the understanding and interpretation of these systems continues to evolve. There is limited available literature with district-scale comparisons and this project aims to provide documentation of similarities and differences in host rocks, veins and alteration distribution and provide recommendations of future research and exploration implications. There are many broad similarities across the four deposits in this study that were observed across the TGB, this includes similar vein textures, vein styles, distribution of veins and correlative vein selvedge alteration assemblages. Next steps for this project include the publication of a supplemental

rock atlas and accompanying geochronological data (Re-Os molybdenum and U-Pb zircon CA-TIMS) age dates. Geochronology data will provide an updated framework and interpretation of regional temporal relationships of the distribution of magmatism and related mineralization in the Selwyn basin throughout the mid-Cretaceous.

Acknowledgments

The author would like to recognize that all of the properties visited as part of this ongoing study are within the Traditional Territory of the First Nation of Na-chö Nyäk Dun. Tiera Naber and Ruby Saban provided appreciable field assistance and support during the field season. Patrick Sack, Alex Brubacher, Rosie Cobbett, David Moynihan and Don Murphy are thanked for providing feedback, discussion and revisions of this paper. Discussions both in the field and offsite with the geology teams at Snowline Gold Corp., Sitka Gold Corp., Victoria Gold Corp. and Banyan Gold Corp., as well as many others, significantly improved and continue to improve, and progress the understanding and direction of this project and future work. Logistical support and good company in all camps was greatly appreciated.

References

Abbott, G., 1997. Geology of the Upper Hart River area, eastern Ogilvie Mountains, Yukon Territory (116A/10, 116A/11). Exploration and Geological Services Division, Yukon, Indian and Northern Affairs Canada, Bulletin 9, 92 p

Abbott, J.G., Gordey, S.P. and Tempelman-Kluit, D.J., 1986. Setting of stratiform, sediment hosted lead-zinc deposits in Yukon and northeastern British Columbia. In: Mineral Deposits of Northern Cordillera, Special Volume 37, J.A. Morin (ed.), Canadian Institute of Mining and Metallurgy, p. 1–18.

Baker, T. and Lang, J.R., 2001. Intrusion-related gold systems: the present level of understanding. Mineralium Deposita, vol. 36, p. 477–489.

Bailey, E.H. and Stevens, R.E., 1960. Selective staining of K-feldspar and plagioclase on rock slabs and thin sections. The American Mineralogist, vol. 45, no. 9-10, p. 1020–1025.

Barbarin, B. and Didier, J., 1992. Genesis and evolution of mafic microgranular enclaves through various types of interaction between coexisting felsic and mafic magmas. Transactions of the Royal Society of Edinburgh Earth Sciences, vol. 83, p. 145-153.

Burrell, H., Haggarty, S.C. and Redmond, D.J., 2024. Rogue project NI 43-101 technical report and mineral resource estimate. Report date July 23, 2024. Effective May 15, 2024.

Cave, B.J., Barnes, S.-J., Pitcairn, I.K., Sack, P.J., Kuikka, H., Johnson, S.C. and Duran, C.J., 2019. Multi-stage precipitation and redistribution of gold, and its collection by lead-bismuth and lead immiscible liquids in a reduced intrusion-related gold system (RIRGS); Dublin Gulch, western Canada. Ore Geology Reviews, vol. 106, p. 28–55, https://doi.org/10.1016/j.oregeorev.2019.01.010.

Cecile, M.P., 1982. The Lower Paleozoic Misty Creek embayment, Selwyn basin, Yukon and Northwest Territories. Geological Survey of Canada, Bulletin 335, 88 p.

Cecile, M.P., Morrow, D.W. and Williams, G.K., 1997. Early Paleozoic (Cambrian to Early Devonian) tectonic framework, Canadian Cordillera. Bulletin of Canadian Petroleum Geology, vol. 45, p. 54–74.

Cernuschi, F., Dilles, J.H., Osorio, J., Proffett, J.M. and Kouzmanov, K., 2024. A reevaluation of the timing and temperature and molybdenum precipitation in porphyry deposits. Economic Geology, vol. 118, p. 931–965.

Cobbett, R.N., Beranek, L.P., Piercey, S.J., Crowley, J.L. and Colpron, M., 2023. Early Ordovician seamounts preserved in the Canadian Cordillera: Implications for the rift history of western Laurentia. Geosphere, vol. 19, no. 5, p. 1421–1451.

Cobbett, R.N., Colpron, M., Crowley, J. L., Cordey, F., Blodgett, R. B. and Orchard, M. J., 2021. Late Devonian magmatism and clastic deposition in the upper Earn Group (central Yukon, Canada) mark the transition from passive to active margin along western Laurentia. Canadian Journal of Earth Sciences, vol. 58, no. 5, p. 471–494

Colpron, M., Israel, S. and Friend, M. (compilers), 2016. Yukon plutonic suites. Yukon Geological Survey, Open File 2016-37, scale 1:750 000.

Colpron, M. and Nelson, J.L., 2011. A digital atlas of terranes for the northern Cordillera. Yukon Geological Survey, www.geology.gov.yk.ca, [December, 2024]; also British Columbia Ministry of Energy and Mines, BCGS GeoFile 2011-11.

Colpron, M., Nelson, J.L. and Murphy, D.C., 2006. A tectonostratigraphic framework for the pericratonic terranes of the northern Canadian Cordillera. In: Paleozoic Evolution and Metallogeny of Pericratonic Terranes at the Ancient Pacific Margin of North America, Canadian and Alaskan Cordillera, M. Colpron and J. Nelson (eds.), Geological Association of Canada Special Paper 45, p. 1–23.

Cook, C., Hulse, D., Rodriguez, G.D.R. and Bianchin, M., 2022. Preliminary economic assessment NI 43-101 technical report on the Brewery Creek project, Yukon Territory, Canada. Prepared for Sabre Gold. Mineral Resource. Effective Date May 31, 2020.

Frost, B.R. and Frost, C.D., 2008. A geochemical classification for feldspathic igneous rocks. Journal of Petrology, vol. 49, p. 1955–1969. https://doi.org/10.1093/petrology/egn054.

Gabrielse, H., Blusson, S.L. and Roddick, J., 1973. Geology of Flat River, Glacier Lake, and Wrigley Lake map-areas, district of Mackenzie and Yukon Territory Part 1: General geology, structural geology and economic geography. Geological Survey of Canada, Department of Energy, Mines and Resources, Memoir 366, 170 p.

Gabrielse, H., Murphy, D.C. and Mortensen, J.K., 2006. Cretaceous and Cenozoic dextral orogen-parallel displacements, magmatism, and paleogeography, north-central Canadian Cordillera. In: Paleogeography of the North American Cordillera: Evidence for and against large-scale displacements, J.W. Haggart, R.J. Enkin, and J.W.H. Monger (eds.), Geological Association of Canada Special Paper 46, p. 255–276.

Goodfellow, W.D., Cecile, M.P. and Leybourne, M.I., 1995. Geochemistry, petrogenesis and tectonic setting of Lower Paleozoic alkalic and potassic volcanic rocks, northern Canadian Cordilleran miogeocline. Canadian Journal of Earth Sciences, vol. 32, p. 1236–1254.

Gordey, S.P., 2013. Evolution of the Selwyn basin region, Sheldon Lake and Tay River map areas, central Yukon. Geological Survey of Canada, Bulletin 599, 176 p.

Gordey, S.P. and Anderson, R.G., 1993. Evolution of the northern Cordilleran miogeocline, Nahanni map area (105I), Yukon and Northwest Territories. Geological Survey of Canada, Department of Energy, Mines and Resources, Memoir 428, 214 p.

Hart, C., 2007. Reduced intrusion-related gold systems. In: Mineral Deposits of Canada: A synthesis of major deposit types, district metallogeny, the evolution of geological provinces, and exploration methods, W.D. Goodfellow (ed.), Geological Association of Canada, Mineral Deposits Division, Special Publication 5, p. 95–112.

Hart, C.J.R., Baker, T. and Burke, M., 2000. New exploration concepts for country-rock-hosted, intrusion-related gold systems: Tintina gold belt in Yukon. In: The Tintina Gold Belt Concepts, Exploration and Discoveries, Cordilleran Exploration Roundup 2000, extended abstract volumes.

Hart, C.J.R., Mair, J.L., Goldfarb, R.J. and Groves, D.I., 2004. Source and redox controls on metallogenic variations in intrusion-related ore systems, Tombstone-Tungsten belt, Yukon Territory, Canada. Transactions of the Royal Society of Edinburgh, Earth Sciences, vol. 95, p. 339–356.

Hart, C., McCoy, D., Goldfarb, R., Smith, M., Roberts, P., Hulstein, R., Bakke, A.A. and Bundtzen, T.K., 2002. Geology, exploration and discovery in the Tintina gold province, Alaska and Yukon. Society of Economic Geologists Special Publication 9, P. 241–274.

Harvey, N., Gray, P., Winterton, J., Jutras, M. and Levy., M., 2023. Technical report Eagle Gold Mine Yukon Territory, Canada. Effective Date December 31, 2022. Report Date April 10, 2023.

Jennings, D.S. and Jilson, G.A., 1986. Geology and sulphide deposits of Anvil Range, Yukon. In: Mineral Deposits of Northern Cordillera, Special Volume 37, J.A. Morin (ed.), Canadian Institute of Mining and Metallurgy, p. 319-361.

Kirk, F.A., 2016. Paragenesis, geochemistry and metallogeny of the Dublin Gulch intrusion-related Au deposit, Yukon Territory, Canada. Unpublished MSc thesis, Memorial University, Newfoundland and Labrador, Canada, 362 p.

Lang, J.R., Baker, T., Hart, C. and Mortensen, J.K., 2000. An exploration model for

intrusion-related gold systems. Society of Economic Geologists, SEG Discovery 2000, no. 40, p. 1–15.

Lindsay, M., 2006. The structural and hydrothermal evolution of intrusion-related gold mineralisation at the Brewery Creek Mine, Yukon, Canada. Unpublished PhD thesis, James Cook University, Australia, 348 p.

MacNaughton, R.B., Moynihan, D.P., Roots, C.F. and Crowley, J.L., 2016. New occurrences of Oldhamia in eastern Yukon, Canada: Stratigraphic context and implications for Cambrian deep-marine biostratigraphy. Ichnos, vol. 23, p. 33–52.

Mair, J.L., Hart, C.J.R., Goldfarb, R.J., O'Dea, M. and Harris, S., 2000. Geology and metallogenic signature of gold occurrences at Scheelite Dome, Tombstone gold belt, Yukon. In: Yukon Exploration and Geology 1999, D.S. Emond and L.H. Weston (eds.), Exploration and Geological Sciences Division, Yukon Region, Indian and Northern Affairs Canada, p. 165–176.

Mair, J.L., Hart, C.J.R. and Stephens, J.R., 2006. Deformation history of the northwestern Selwyn basin, Yukon, Canada: Implications for orogeny evolution and mid-Cretaceous magmatism. Geological Society of America Bulletin, vol. 118, p 304–323.

Marsh, E.E., Goldfarb., R.J., Hart, C.J.R. and Johnson, C.A., 2003. Geology and geochemistry of the Clear Creek intrusion-related gold occurrences, Tintina gold province, Yukon, Canada. Canadian Journal of Earth Science, vol. 40, p. 681–699.

Marsh, E.E., Hart, C.J.R., Goldfarb, R.J. and Allen, T.L., 1999. Geology and geochemistry of the Clear Creek gold occurrences, Tombstone gold belt, central Yukon Territory. In: Yukon Exploration and Geology 1998, C.F. Roots and D.S. Emond (eds.), Exploration and Geological Services Division, Yukon, Indian and Northern Affairs Canada, p. 185–196.

McDonough, W.F. and Sun, S., 1995. The composition of the Earth. Chemical Geology, vol. 120, p. 223–253.

Moynihan, D.P., Strauss, J.V., Nelson, L.L. and Padget, C.D., 2019. Upper Windermere Supergroup and the transition from rifting to continent-margin sedimentation, Nadaleen River area, northern Canadian Cordillera. Geological Society of America Bulletin, vol. 131, no. 9-10, p. 1673-1701.

Murphy, D.C. 1997. Geology of the McQuesten River region, northern McQuesten and Mayo map area, Yukon Territory. Exploration and Geological Services Division, Yukon, Indian and Northern Affairs Canada, Bulletin 6, 122 p.

Murphy, D.C., Mortenson, J.K., Piercey, S.J., Orchard, M.J. and Gehrels, G.E., 2006. Mid-Paleozoic to early Mesozoic tectonostratigraphic evolution of Yukon-Tanana and Slide Mountain terranes and affiliated overlap assemblages, Finlayson Lake massive sulphide district, southeastern Yukon. In: Paleozoic Evolution and Metallogeny of Pericratonic Terranes at the Ancient Pacific Margin of North America, Canadian and Alaskan Cordillera, M. Colpron and J. Nelson (eds.), GAC SP45, p. 75-105.

Piercey, S.J., Nelson, J.L., Colpron, M., Dusel-Bacon, C., Simard, R.-L. and Roots, C.F., 2006. Paleozoic magmatism and crustal recycling along the ancient Pacific margin of North America, northern Cordillera. In: Paleozoic Evolution and Metallogeny of Pericratonic Terranes at the Ancient Pacific Margin of North America, Canadian and Alaskan Cordillera, M. Colpron and J.L. Nelson (eds.), Geological Association of Canada Special Paper 45, p. 281–322.

Rasmussen, K.R., 2013. The timing, composition, and petrogenesis of syn- to post-accretionary magmatism in the northern Cordilleran miogeocline, eastern Yukon and southwestern Northwest Territories. Unpublished PhD thesis, University of British Columbia, Vancouver, British Columbia, Canada, 810 p.

Rock, N.M.S., Groves, D.I., Perring, C.S. and Golding, S.D., 1989. Gold, lamprophyres, and porphyries: What does their association mean? The Geology of Gold Deposits: The Perspective in 1988, Society of Economic Geologists, R.R. Keays, W.R.H. Ramsay and D.I. Groves (eds.), p. 609–625.

Roots, C.F., 1997. Geology of the Mayo map area, Yukon Territory (105M). Indian and Northern Affairs Canada, Exploration and Geological Services Division, Yukon, Bulletin 7, 82 p.

Roots, C.F., 1998. Progress report on bedrock geology of Lansing map area, central Yukon Territory. Geological Survey of Canada, Current Research 1998-A, p. 19–28.

Roots, C.F., 2003. Bedrock geology of Lansing Range map area (NTS 105N), central Yukon (1:250 000 scale). Yukon Geological Survey, Energy Mines and Resources, Government of Yukon, Geoscience Map 2003-1; also Geological Survey of Canada, Open File 1616.

Rusk, B.G., Reed, M.H. and Dilles, J.H., 2008. Fluid inclusion evidence for magmatic-hydrothermal fluid evolution in the porphyry copper-molybdenum deposit at Butte, Montana. Economic Geology, vol. 103, p. 307–344.

Sack, P.J., Kruse, S. and Ferraro, D., 2018. Gold occurrences on the Plateau South property (Yukon MINFILE 105N 034, 035, 036), central Yukon. In: Yukon Exploration and Geology Overview 2017, K.E. MacFarlane (ed.), Yukon Geological Survey, p. 75–91.

Seedorff E., Dilles, J.H., Proffett Jr., J.M., Einaudi, M., Zurcher, L., Stavast, W.J.A., Johnson, D.A. and Barton, M.D., 2005. Porphyry deposits: Characteristics and origin of hypogene features. Economic Geology 100th Anniversary Volume, p. 251–298.

Selby, D., Creaser, R., Heaman, L. and Hart, C., 2003. Re Os and U Pb geochronology of the Clear Creek, Dublin Gulch and Mactung deposits, Tombstone gold belt, Yukon, Canada: absolute timing relationships between plutonism and mineralization. Canadian Journal of Earth Sciences, vol. 40, p. 1839–1852.

Sillitoe, R.H., 2010. Porphyry copper systems. Economic Geology, vol. 105, no. 1, p. 3–41, https://doi.org/10.2113/gsecongeo.105.1.3.

Simpson, R., 2023. Clear Creek property, RC Gold project, NI 43-101 Technical Report, Dawson Mining District, Yukon Territory.

Stephens, J.R., Mair, J.L., Oliver, N.H.S., Hart, C.J.R. and Baker, T., 2004. Structural and mechanical controls on intrusion-related deposits of the Tombstone gold belt., Yukon, Canada, with comparisons to other vein-hosted ore-deposit types. Journal of Structural Geology, vol. 26, issues 6-7, p. 1025–1041.

Stephens, J.R., Oliver, N.H.S., Baker, T. and Hart, C.J.R., 2000. Structural evolution and controls on gold mineralization at Clear Creek, Yukon. In: Yukon Exploration and Geology 1999, D.S. Emond and L.H. Weston (eds.), Exploration and Geological Sciences Division, Yukon Region, Indian and Northern Affairs Canada, p. 151–163.

Vernon, R.H., 1984. Microgranitoid enclaves in granites—globules of hybrid magma quenched in a plutonic environment. Nature, vol. 309, p. 438–439.

Whitney, D.L. and Evans, B.W., 2010. Abbreviations for names of rock-forming minerals. American Mineralogist, vol. 95, p. 185–187.

Yukon Geological Survey, 2022. Yukon MINFILE, a database of mineral occurrences. Yukon Geological Survey, https://data.geology.gov.yk.ca/Occurrences/ [accessed December 1, 2024].

Yukon Geological Survey, 2022. Yukon digital bedrock geology. Yukon Geological Survey, https://data.geology.gov.yk.ca/Compilation/3 [accessed December 1, 2024].

Appendices

Appendix A

Alteration box plots. Ishikawa alteration index versus chlorite-carbonate-pyrite index highlight alteration from fresh rock in whole-rock samples. Unaltered samples should plot within their respective mafic rock equivalents. Outlier samples from whole-rock data are the two lamprophyres from the Blackjack and Eiger deposits, and most samples from Brewery Creek. This plot was first designed for use in volcanic-hosted massive sulphide (VHMS) deposits and does not include any direct measure of the intensity of quartz or silica alteration.

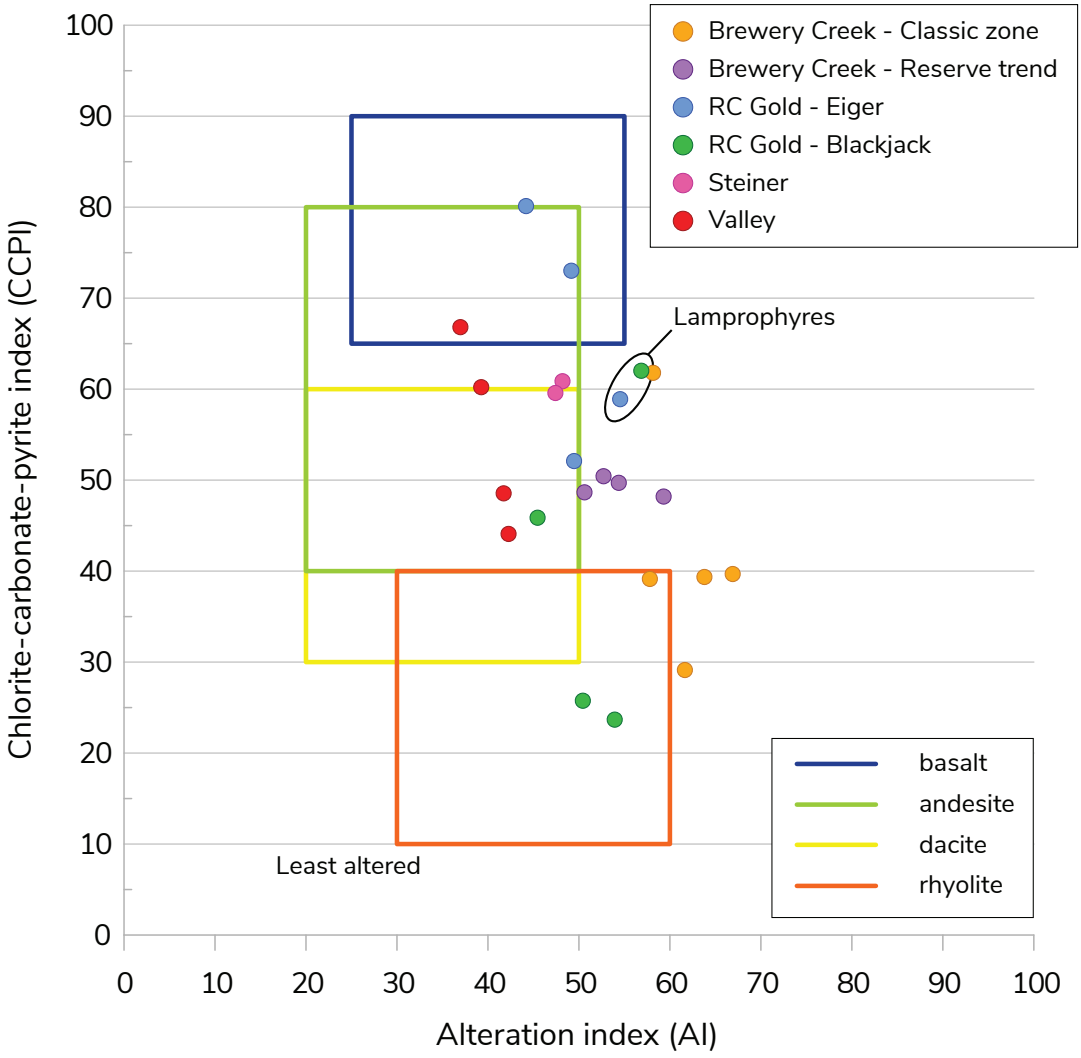

Appendix B (digital)

Raw data from whole-rock geochemistry.

Appendix C

Frost and Frost (2008) classification of all representative whole-rock samples across the four deposits.